Results in Engineering 25 (2025) 104465

Contents lists available at ScienceDirect

Results in Engineering

journal homepage: www.sciencedirect.com/journal/results-in-engineering

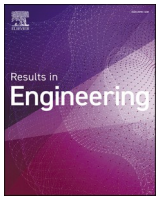

Research paper

Room temperature tribological properties of molybdenum-titanium-zirconium (TZM) in metal forming processes

Hamed Aghajani Derazkola [a,b,c,*], Leonardo Pelcastre [c], Eduardo Garcia [a], Pello Jimbert [d], Jens hardell [c]

[a] Department of Mechanics, Design and Industrial Management, University of Deusto, 48007, Bilbao, Spain
[b] Nonlinear Solid Mechanics, Faculty of ET, University of Twente, Drienerlolaan 5, 7522 NB, Enschede, The Netherlands
[c] Department of Applied Physics and Mechanical Engineering, Luleå University of Technology, Luleå, 97187, Sweden
[d] Faculty of Engineering Bilbao, University of the Basque Country, UPV/EHU, Bilbao, Spain

ARTICLE INFO

Keywords:
TZM
AISI 430 steel
Wear mechanism
Contact temperature

ABSTRACT

This study investigate the effects of temperature on the tribological properties of Titanium-zirconium-molybdenum (TZM). TZM alloy was subjected to sliding contact against AISI 430 steel counterparts at varying temperatures. The results shows, the coefficients of friction (COF) at interface were 0.77, 0.75, 0.71, and 0.69, in the case of 25 °C, 300 °C, 600 °C, and 900 °C test temperatures. The presence of MoO_3 and Mo_9O_{26} phases suggested the wear resistance and decreasing COF at high temperature. Temperature is a critical factor influencing material transfer between TZM and AISI 430 steel. The primary TZM wear mechanism at 25 °C involved scratching, surface deformation, and local cracks, while elevated temperatures near 900 °C intensified material adhesion phenomena with a surface shearing effect on the TZM surface after the trotest.

1. Introduction

In the realm of materials science and engineering, the development and utilization of advanced materials for industrial applications play a pivotal role in enhancing manufacturing efficiency, product quality, and overall economic growth [1]. Molybdenum-titanium-zirconium (TZM) is one such remarkable material that has garnered considerable attention due to its exceptional properties and its significance as a forming tool in various metal forming processes [2]. TZM is a refractory metal alloy that is renowned for its unique combination of high-temperature strength, excellent thermal conductivity, and remarkable resistance to thermal shock [3]. Composed primarily of molybdenum (Mo), titanium (Ti), and zirconium (Zr), TZM exhibits superior mechanical and thermal properties, rendering it highly suitable for demanding industrial applications, particularly in the field of metal forming [4,5]. The incorporation of titanium and zirconium enhances TZM's mechanical properties, resulting in improved tensile strength, hardness, and durability [6,7]. TZM can be machined into various tool geometries for customized forming processes. Its exceptional properties make it ideal for metal forming applications such as forging, rolling, extrusion, and stamping [8,9]. TZM's high-temperature stability and mechanical robustness render it an ideal choice for shaping and transforming metallic materials under high pressures or high temperatures [10,11]. The operational temperature indeed has a substantial impact on the tool life of TZM during metal forming processes. Elevated temperatures can lead to thermal softening and reduced mechanical strength, affecting the tool's ability to withstand deformation and wear [12]. Conversely, operating at excessively low temperatures might lead to embrittlement and increased susceptibility to cracking [13]. Therefore, optimizing the operating temperature within the material's suitable range is essential to maximize the tool's life and performance. Wear analysis of TZM as a forming tool involves an in-depth examination of its wear mechanisms, modes, and characteristics during metal forming processes. AISI 430 steel is a ferritic stainless steel known for its versatile properties and wide-ranging applications. AISI 430 steel is primarily composed of iron, with notable amounts of chromium, providing it with commendable corrosion resistance and mechanical strength [14]. In various components, AISI 430 steel finds extensive utilization as sheet material due to its exceptional combination of attributes. These sheets are commonly employed in industries such as automotive, architecture, and household appliances, where its robustness, corrosion resistance, and aesthetic appeal contribute to its efficacy [15]. The deformation of AISI 430 steel

* Corresponding author.
E-mail address: h.aghajaniderazkola@utwente.nl (H. Aghajani Derazkola).

https://doi.org/10.1016/j.rineng.2025.104465
Received 27 December 2024; Received in revised form 11 February 2025; Accepted 23 February 2025
Available online 27 February 2025

Table 1
Chemical and mechanical properties of TZM at room temperature.

Chemical Composition (ASTM B387)					
Mo (Wt.%)	Ti (Wt.%)		Zr (Wt.%)		
Balance	0.4 %–0.55 %		0.06 %–0.12 %		
Mechanical properties					
Tensile Strength	Yield Strength	Elongation	Hardness	Melting point	Density
≥585 MPa	≥515 MPa	≥1.5 %	220–280 HV_{10}	2610 °C	10.2 g/cm^3

sheets is a multifaceted process, encompassing room, warm, and hot forming techniques [16]. In room forming, the sheets can be plastically deformed at ambient temperatures, enabling intricate shaping and customization [17]. Warm forming involves deformation at intermediate temperatures, exploiting the material's improved ductility while maintaining a balance between formability and mechanical properties [18].

Hot forming, conducted at elevated temperatures, leverages the heightened malleability of AISI 430 steel to achieve complex geometries that might be unattainable through cold or warm forming. Crucially, the choice of tool material is paramount in sheet deformation processes. Its exceptional mechanical strength, high-temperature stability, and superior wear resistance make it a promising candidate for deforming AISI 430 steel across various temperature ranges. Whether in room, warm, or hot forming scenarios, the TZM alloy holds the potential to serve as an effective tool, facilitating precise and efficient sheet deformation. The TZM tool can be utilized in diverse forming processes spanning from ambient to elevated temperatures. However, the frictional characteristics and wear mechanisms exhibited by the TZM tool under such conditions have not been previously explored. Consequently, the objective of this paper is to analyze the friction and wear behaviors of the TZM tool when interfacing with AISI 430 steel at a range of temperatures, corresponding to various metal forming conditions. To achieve this, the TZM tool was positioned at room temperature and coupled with AISI 430 steel, a deformable material subjected to varying temperatures, with the aim of comprehending the underlying tribological properties.

2. Methodology

2.1. Raw materials

In this study, the TZM alloy was chosen as the tool, and AISI 430 steel was selected as the deformable body. For this reason, the pin was made

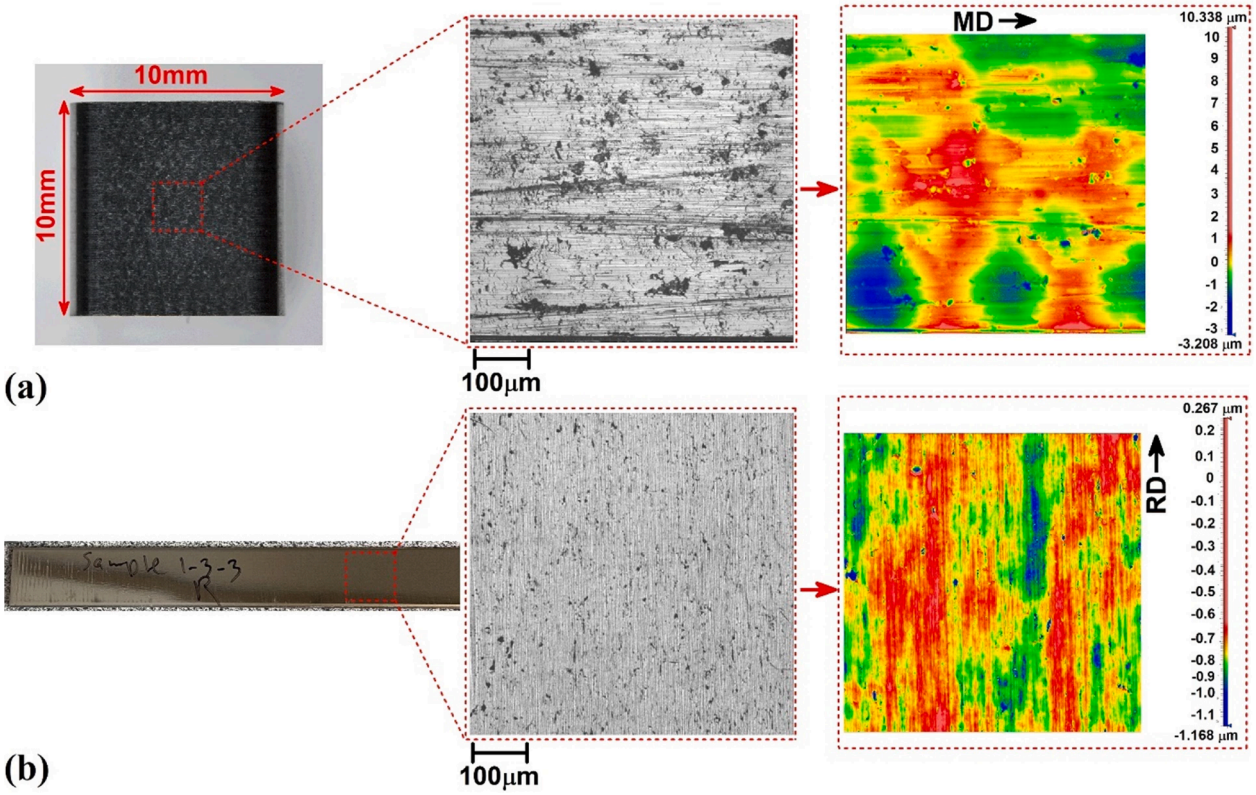

Fig. 1. (a) image of TZM pin with surface topography, (b) image of AISI 430 strip and surface topography.

Table 2
Chemical and mechanical properties of AISI 430 steel.

Chemical Composition (ASTM B387)						
C(Wt.%)	Cr (Wt.%)	Mn (Wt.%)	P (Wt.%)	S (Wt.%)	Si (Wt.%)	Fe (Wt.%)
0.08	16–18		1.00	0.04	1.00	Balance
Mechanical properties						
Ultimate Tensile Strength		Yield Strength		Elongation	Hardness	Melting point
480–600MPa		280MPa		20 %	162HV	1520 °C

Table 3
Testing conditions and sample names.

Sample Name	Applied load	Sliding velocity	Pin Temperature	Strip Temperature	Contact Temperature
I	600N	250mm/min	25 °C	25 °C	25 °C
II	600N	250mm/min	25 °C	300 °C	110 °C
III	600N	250mm/min	25 °C	600 °C	195 °C
IV	600N	250mm/min	25 °C	900 °C	300 °C

by TZM, and the strip was AISI 430 steel. In this case, the tribological properties of TZM could be evaluated. The TZM alloy was precisely cut into a rectangular cube by a milling machine measuring 10 mm × 10 mm × 20 mm, facilitating a standardized platform for experimentation. The sides of the pin had a 1.5 mm radius fillet, which led to a 7 mm × 10 mm real contact area on the surface of TZM pins. Table 1 comprehensively elucidates the chemical and mechanical properties of the utilized TZM alloy. Furthermore, a 2 mm diameter aperture has been meticulously drilled on the pin, serving as a receptacle for thermocouples, a critical element for precise temperature measurements. The thermocouple had 0.5 mm distance with top surface of TZM pin. The pin surface, accentuated by its surface roughness, is illustrated in Fig. 1a, offering a visual depiction that augments the topographical attributes. The TZM pins prepared by milling machining and milling direction (MD)

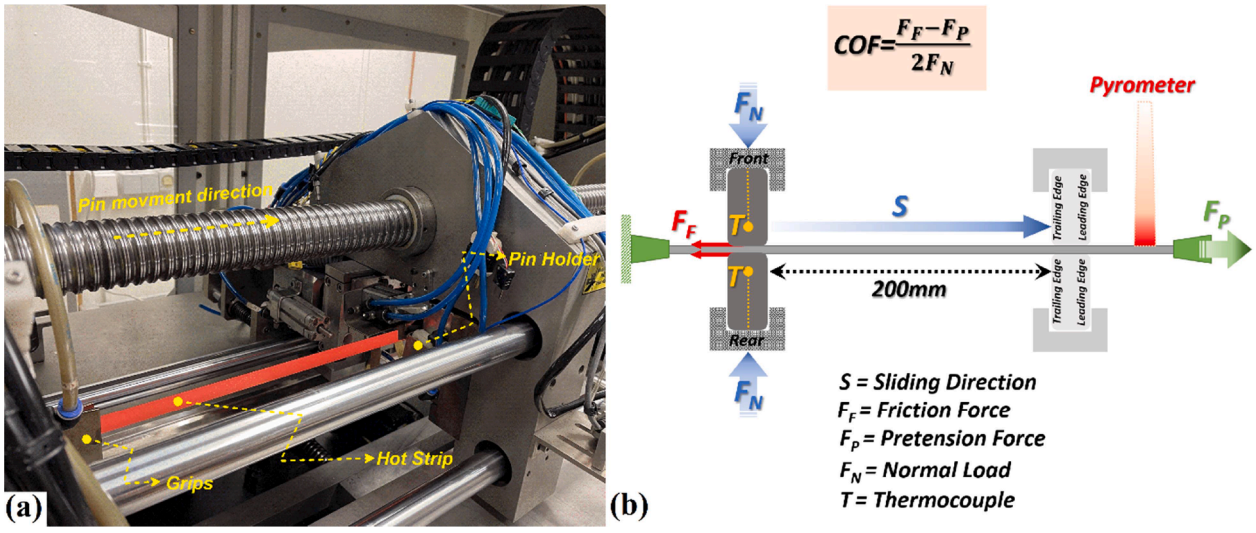

Fig. 2. (a) Image of hot friction test machine used in this study, (b) schematic view of operation mechanism of hot friction test machine.

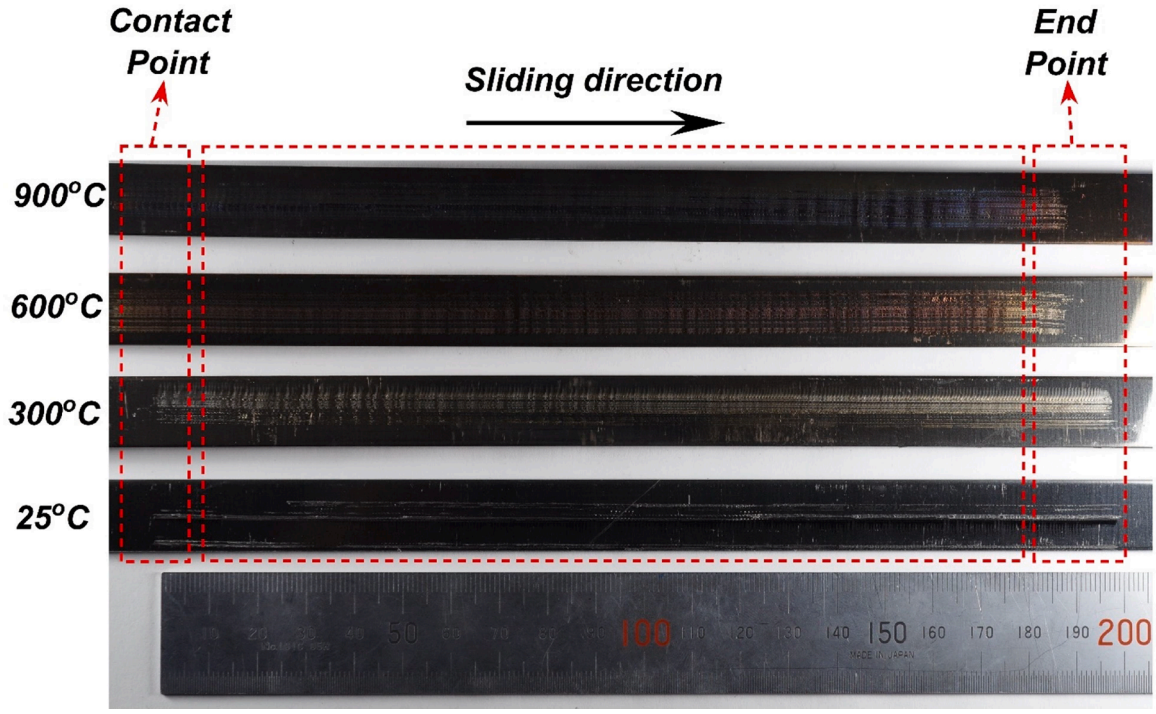

Fig. 3. Optical image of tested strips at various testing temperatures.

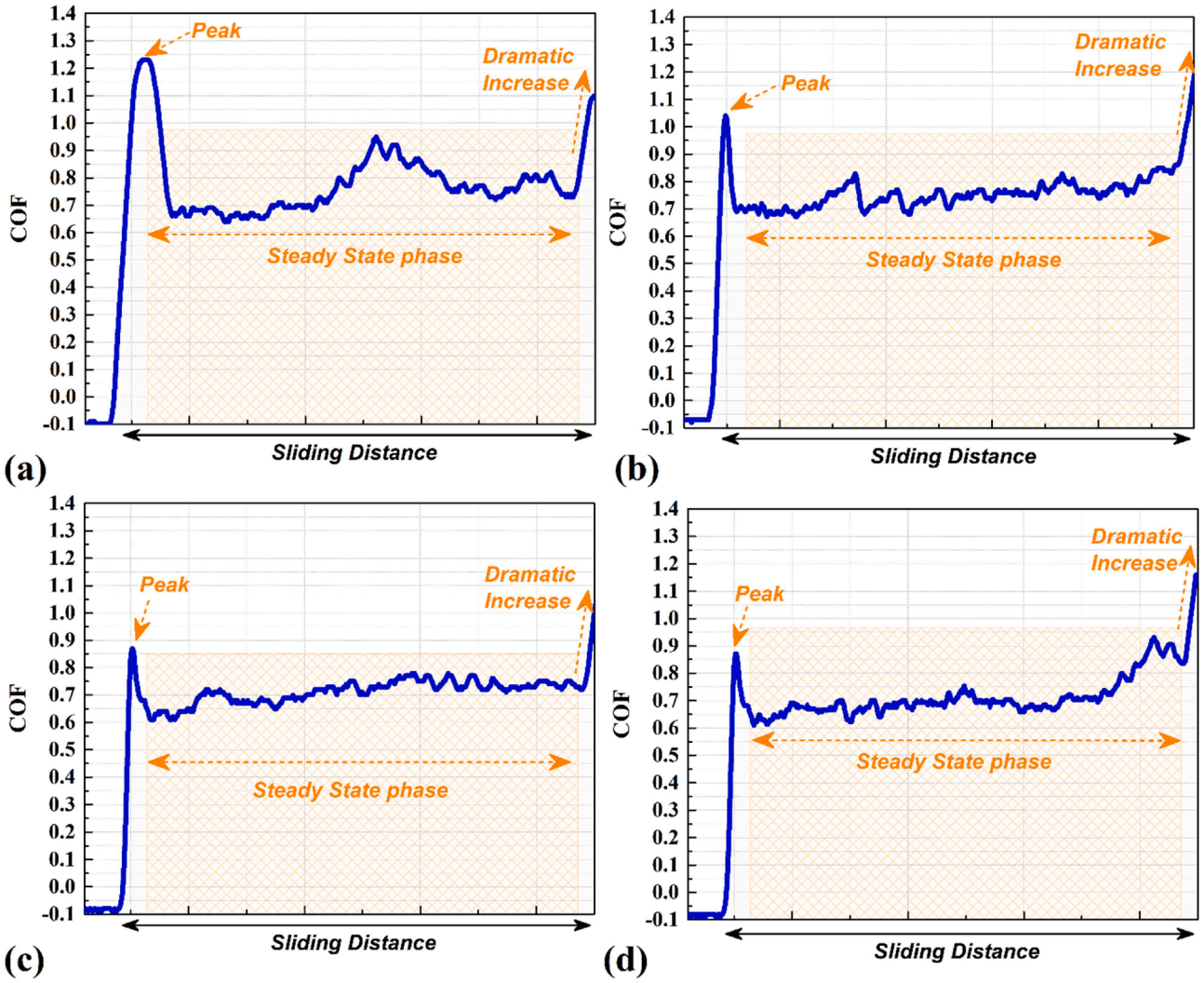

Fig. 4. COF graphs of TZM pin against AISI 430 strip at (a) 25 °C, (b) 300 °C, (c) 600 °C, and (d) 900 °C. Sliding distance shows 200 mm in all cases.

are depicted on the pin's surface topography. The average Sa and Sq of TZM pin were 1.641 ± 0.05 μm and 2.448 ± 0.04 μm, respectively. AISI 430 steel has been selected as the strip component, taking the form of strips that were derived from cold-rolled sheets. These strips, measuring 1.5 mm × 20 mm × 1000 mm, were cut perpendicular to the rolling direction (the 1000 mm length of strip was in rolling direction), ensuring uniformity and consistent dimensions. Detailed in Table 2, the chemical and mechanical properties of the chosen AISI 430 steel strip are given. The average Sa and Sq of the AISI 430 steel strip were 0.512 ± 0.02 μm and 1.001 ± 0.06 μm, respectively. The pins and strips surfaced (As-received) evaluated by Zygo NewView 9000 light optical interferometer. Fig. 1b indicates the surface of the strip, shedding light on its inherent surface roughness.

2.2. Friction test equipment and procedure

A hot strip drawing tribometer (Ducom TR 20M-47, India) was employed to conduct tribological tests, allowing for the manipulation of sliding velocities, strip temperatures, and applied loads. The tests involved the interaction between TZM pins and pristine, unworn AISI 430 steel strips. The AISI 430 steel strip was securely positioned and clamped at both ends using machine grips. To replicate the AISI 430 forming process under different conditions, two applied loads and three distinct temperatures were chosen, corresponding to room, warm, and hot environments. Detailed testing conditions are provided in Table 3. The heating process utilized resistive heating, emulating diverse heat cycles. The AISI 430 strip was maintained under positive pre-tension through a pneumatic cylinder while its temperature was monitored using a pyrometer. In the case of pins, the belt resistance heaters increased the temperature of the pins. The pin thermal changes were controlled by thermocouples that were installed inside the pins. Two TZM pins were integrated into a movable tool assembly driven by a ball screw. These pins were pressed against opposing sides of the strip with the assistance of a pneumatic bellow. The sliding distance was set at 200 mm, and each experimental condition was replicated three times. An illustration of the utilized hot strip drawing tribometer can be observed in Fig. 2a. The friction force was measured using a strain gauge force transducer. Coulomb's friction law determined the coefficient of friction in this hot strip drawing tribometer. A diagram depicting the various components, forces, and movements within the hot strip drawing tribometer is presented in Fig. 2b. Throughout the tests, variations in temperature (at the beginning of test) within the pins were monitored using thermocouples, and these readings were subsequently documented and presented as contact temperature in Table 3. The applied load and sliding velocity were selected as process parameters suitable for high-temperature metal forming with a high strain rate, such as the teal piercing process. It is important to note that the contact temperature values listed in Table 3 may not precisely represent the temperatures at the interface area. Rather, these values serve as approximations that can be considered proximate to the actual temperatures experienced.

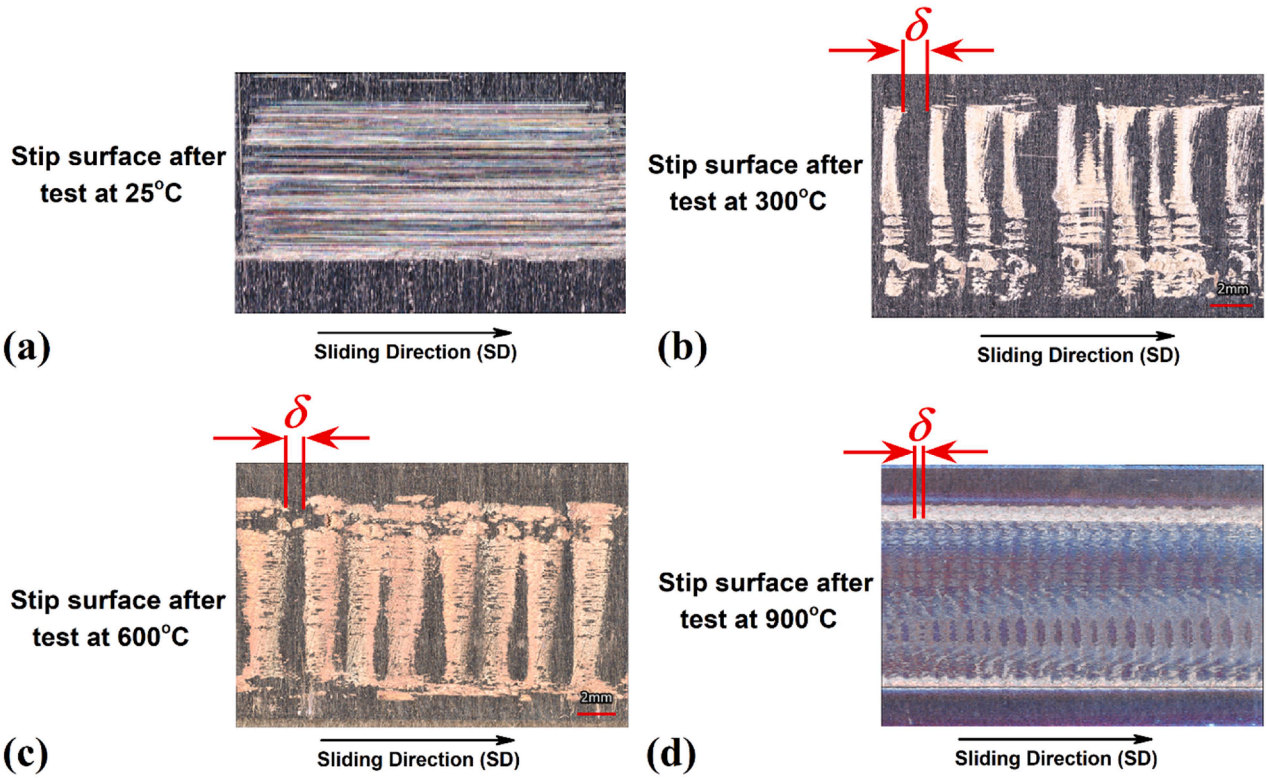

Fig. 5. Optical images from AISI 430 strip that tested at (a) 25 °C, (b) 300 °C, (c) 600 °C, and (d) 900 °C (The images are taken from middle of strip (100 mm) after tribotest).

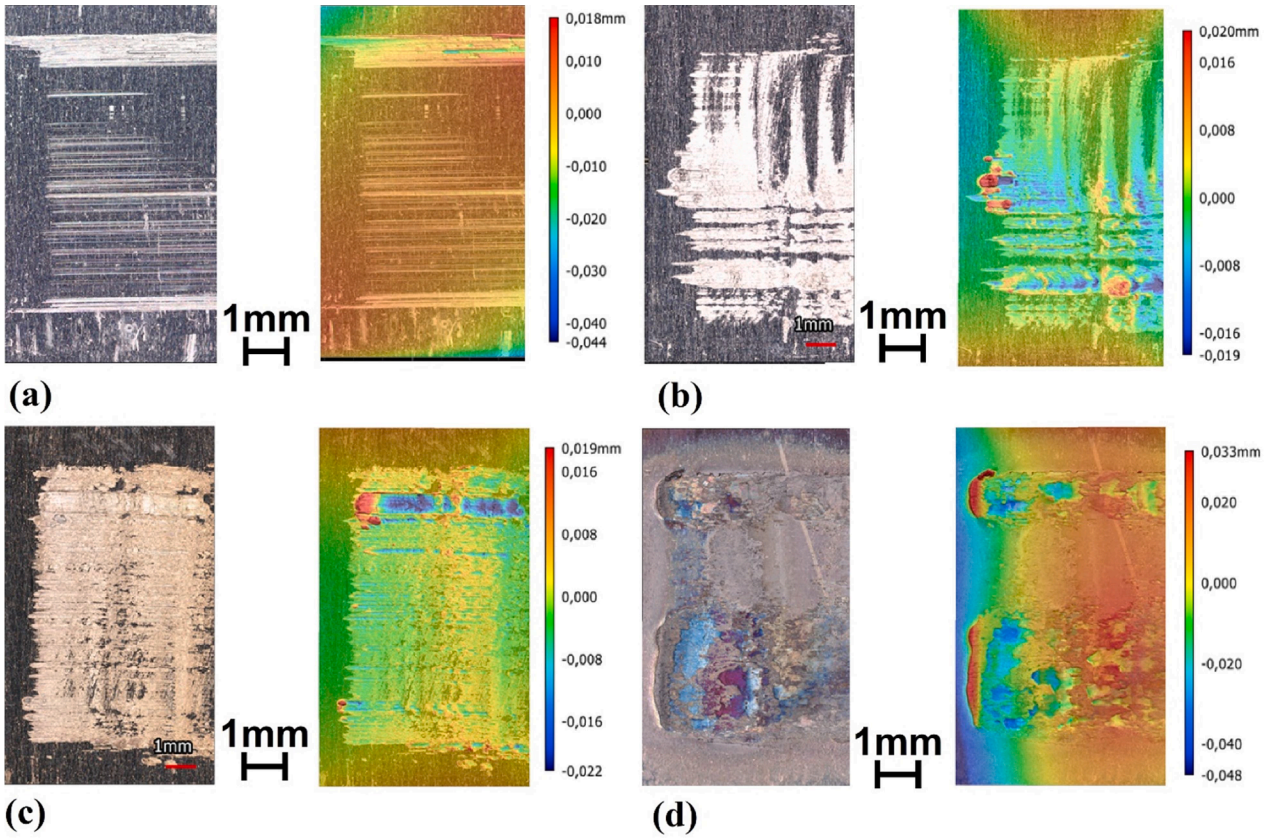

Fig. 6. Optical and profilometry images from AISI 430 strip that tested at (a) 25 °C, (b) 300 °C, (c) 600 °C, and (d) 900 °C.

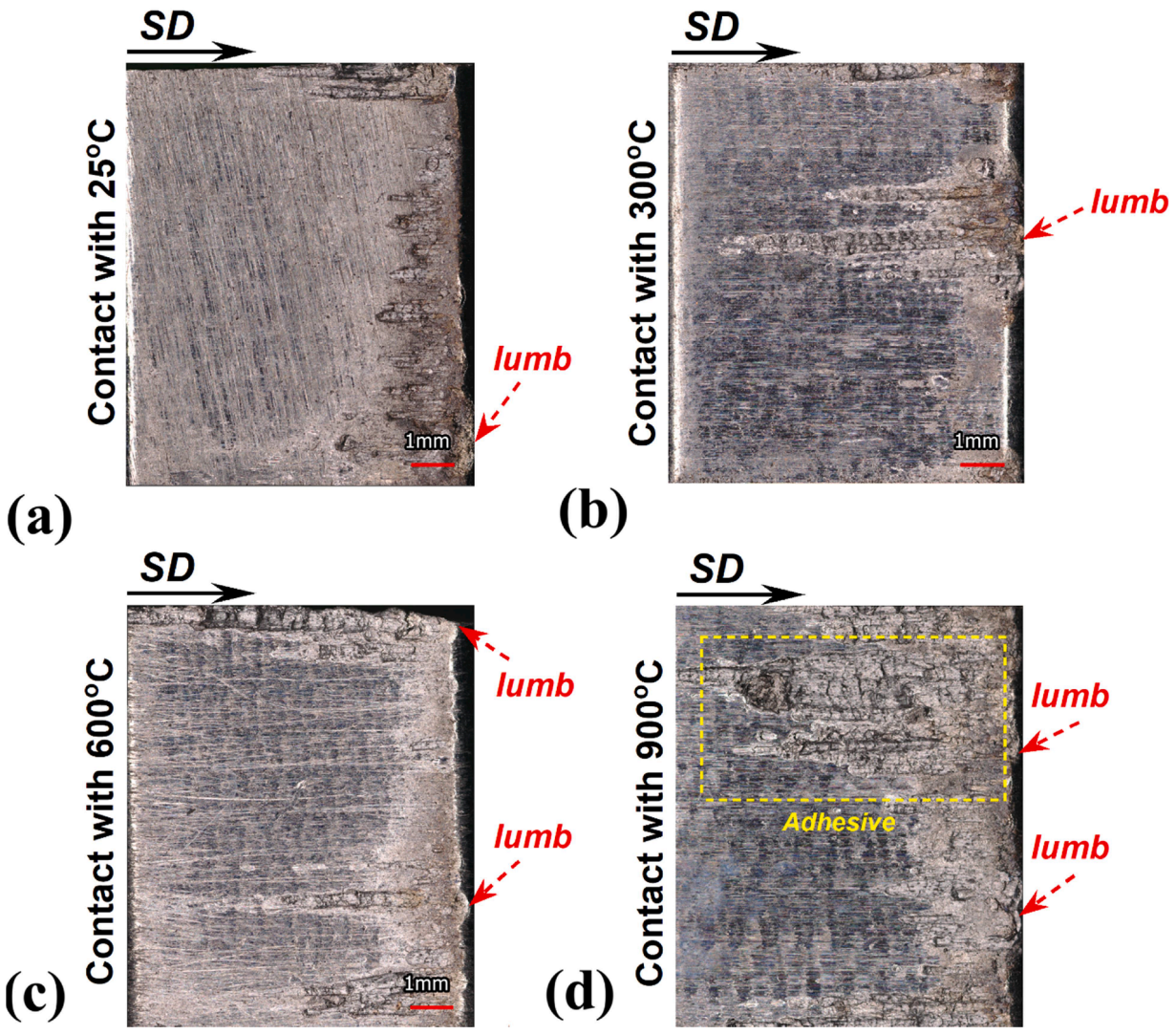

Fig. 7. Optical and profilometry images from TZM pins that tested against AISI 430 strip at (a) 25 °C, (b) 300 °C, (c) 600 °C, and (d) 900 °C.

2.3. Characterization

The surface topography of the pins was assessed using the Keyence VR 5200 wide-area 3D measurement system (KEYENCE INTERNATIONAL,BELGIUM). The Zygo NewView 9000 light optical interferometer (Zygo, USA) was utilized to examine high-magnification topography and damage characteristics. A scanning electron microscope (SEM) (Jeol JSM-IT300, Japan) equipped with energy dispersive spectroscopy (EDS) was employed to gain a deeper insight into the friction and wear mechanisms. EDS (Aztec, Oxford Instruments, UK) was employed to investigate material transfer between the pin and strip materials. The acceleration voltage used for SEM surface analysis was set at 20 kV.

3. Results and discussions

3.1. Analysis of friction coefficient

This friction test procedure involves three distinct stages. The first stage is the contact point and loading of the pins, where the TZM pins make initial contact with the AISI 430 steel (strip). At this point, the strip material and the pin are brought into contact, and the interaction between them begins. Following the loading of the pins, the loading head starts moving the TZM pins forward along the AISI 430 steel strip. This zone can be referred to as the sliding-direction zone. In this stage, the TZM pins are in motion, and frictional forces between the pin and the strip material come into play [19]. The change in frictional behavior as the pins move along the strip can provide valuable insights into how the materials interact at the specific temperatures. The final stage can be attributed to the end-point zone when the friction test is completed. This phase represents the conclusion of the test, and the data collected in this zone helps in understanding how the frictional behavior stabilizes or changes as the pins reach the end of the strip. Fig. 3, which depicts the three zones on the strips tested at different temperatures (25 °C, 300 °C, 600 °C, and 900 °C), offers a visual representation of the strip after the test. The images clearly show the progression of the test procedure, and the distinct zones identified are visible in the images. The difference in the color of the strips corresponding to different temperatures provides a convenient way to correlate the visual data with temperature variations.

The Coefficient of Friction (COF) results at 25 °C, 300 °C, 600 °C, and 900 °C, are shown in Figs. 4a, 4b, 4c, and 4d. The tribotests were stable and repeatable for all tested conditions. These graphs exhibit a distinctive pattern. The COF graph has an initial peak, followed by a steady state phase and a dramatic increase towards the end of the test. This pattern is consistent across all temperature conditions and can be attributed to the distinct phases of the friction test. The initial peak corresponds to the contact point, where the pins first contact the AISI 430 strip and transition from static to dynamic friction.. The steady-state

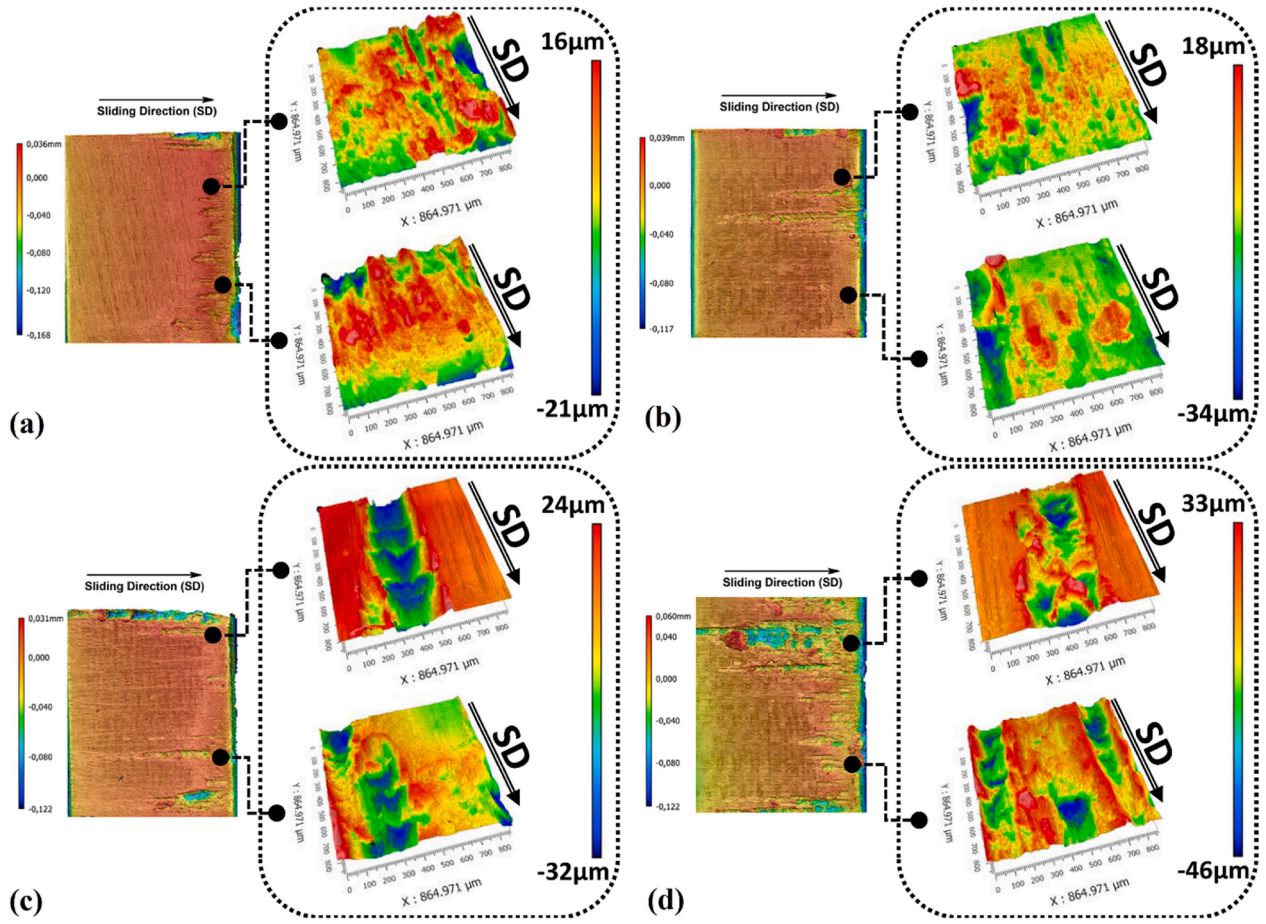

Fig. 8. 3D profilometry results from Surface of (a) ample I, (b) Sample II, (c) Sample III, and (d) sample IV.

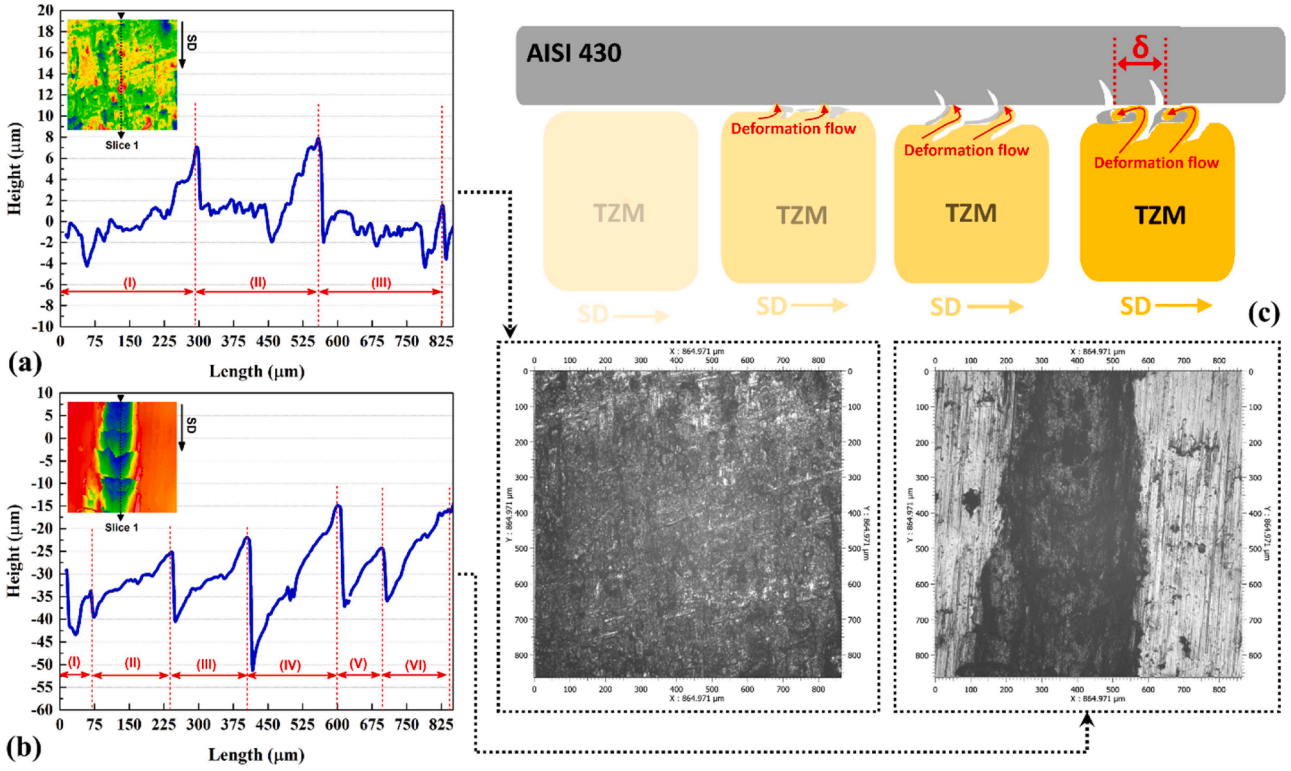

Fig. 9. 3D profilometry results from surface roughness of (a) ample I and (b) Sample IV. (c) The schematic view of formation of (δ) at surface of AISI 430 strip.

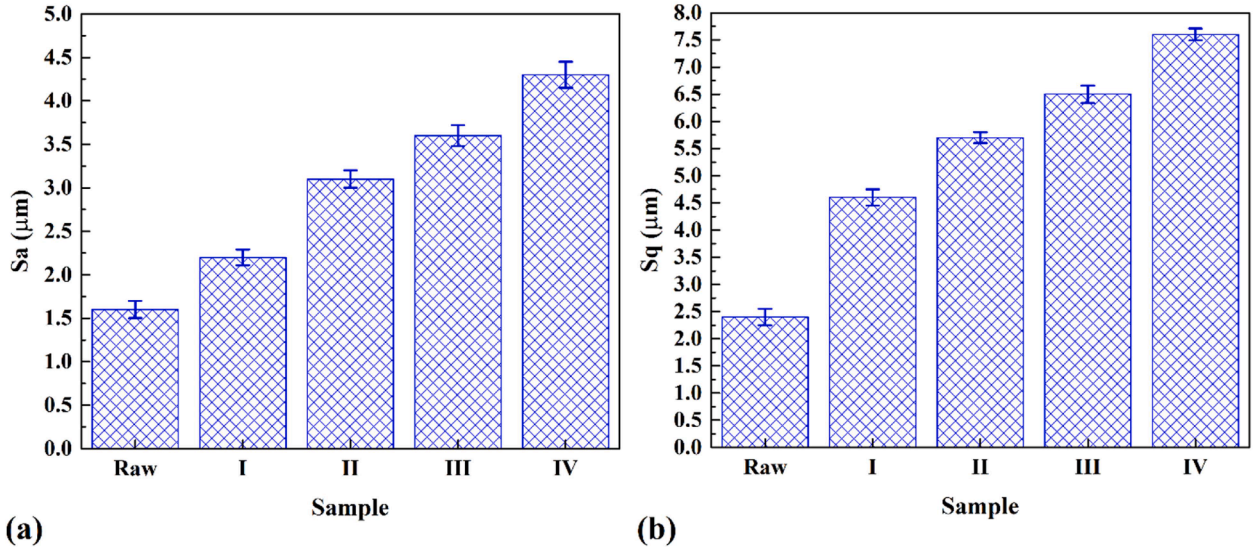

Fig. 10. (a) Sa and (b) Sq results of TZM pins after the test.

phase is recorded during the sliding phase (that was 200 mm), where friction reaches a relatively stable level as the pins move along the Strip. The dramatic increase at the end reflects the endpoint phase, indicating that friction increases as the test nears completion. These distinct phases are a hallmark of the friction testing process. The steady-state phase's mean value is recorded as each case's COF. Due to the obtained results, the COF of TZM in counter with AISI 430 steel were 0.77, 0.75, 0.71, and 0.69, in the case of 25 °C, 300 °C, 600 °C, and 900 °C test temperatures, respectively. This observation suggests higher temperatures reduce friction between TZM and AISI 430 steel [20].

The increased temperature may result in the materials becoming more ductile, or the surfaces of the materials may undergo changes in their mechanical properties or microstructure at elevated temperatures, affecting the interaction between them [21]. The mean values of the COF are collected based on results during the steady-state phase for each temperature condition. The COF decreases as the temperature of the test strip rises. These results suggest that higher temperatures significantly influence the frictional behavior of TZM in contact with AISI 430 steel. The results show that the steady-state phase in all samples was uneven. At 25°, the presence of debris affects the friction graph, causing fluctuations. The COF graphs have fluctuations and a wavy form. These fluctuations may be indicative of variations in friction as the pins move along the Strip, possibly due to local surface irregularities or variations in material properties [22]. The steady-state phase of COF is smothered in the higher temperature of the AISI 430 strip. The COF graphs at 25 °C temperature have more fluctuation compared to other cases.

3.2. AISI 430 steel surface analysis

The images of the Strip surfaces at 25 °C, 300 °C, 600 °C, and 900 °C conditions, as shown in Fig. 5a–d, respectively. The test surface at 25 °C shows uniform scratches, indicating abrasion and debris formation at the beginning and during of the tribotest.

The fluctuation profile on the strip surfaces suggests that the contact between the pins and the strip is not uniform. This non-uniform contact can lead to variations in friction and may be responsible for the fluctuations observed in the COF graphs. The "jumping" phenomenon seen on the strips' surface is shown by $\ddot{\delta}$. This phenomenon could indicate intermittent contact between the TZM pin and the AISI 430 strip surface. Interestingly, the non-contact area decreases as the strip temperature increases, suggesting that higher temperatures may improve the contact between the TZM pin and the AISI 430 trip. The thickest δ is recorded in the 300 °C strip case, and the thinner case is seen in 900 °C. The jumping behavior of TZM against AISI 430 steel is considered before, but not fully understood. It seems the starting contact point can affect this surface pattern on AISI 430 steel strips. The start points of TZM pins at Samples I, II, III and IV are presented in Fig. 6a–d, respectively.

In general, different materials exhibit varying mechanical and thermal properties. As the temperature increases, the material properties of both the TZM pin and the AISI 430 strip may change [23,24]. For example, there could be alterations in hardness, elastic modulus, or thermal expansion coefficients at higher temperatures. The obtained results indicated that the first contact significantly impacts the surface of the AISI 430 steel strip during sliding movements. As can be seen in Fig. 6, with increasing the strip temperature, the deformation in the AISI 430 steel side rises. On the other hand, the contact temperature between TZM and AISI 430 is increased as well. In this case, the TZM pin will be more softened [25], and this phenomenon increases the possibility of abrasive wear at room temperature and adhesive wear and wear debris generation during sliding movement from 300 °C and higher temperature.

3.3. TZM pin surface analysis

Following the completion of the test, a comprehensive surface analysis was conducted on the TZM pins. The obtained results are depicted in Fig. 7a–d, showcasing the surface alterations of TZM pins subjected to strip temperatures of 25 °C, 300 °C, 600 °C, and 900 °C, respectively. Observable modifications were identified across all TZM pins, with a distinct focus on the leading edge, extending towards the trailing edge, albeit more prominently at the leading edge. These findings suggested the occurrence of lumb transfer phenomena at the forefront of the pins. This phenomenon was likely attributed to the pins' leading edge penetrating the AISI 430 steel strip, intensifying contact pressure in that region. It has been shown that an uneven pressure distribution near the leading edge (In this tribo-system) led to the accumulation of wear particles at the center of the pin's leading edge after a certain sliding distance [26]. The tribo-system became increasingly unstable once the transferred material at the leading edge reached a critical level.

The results obtained from the 3D profilometry images of the TZM pins subjected to various strip temperatures (25 °C, 300 °C, 600 °C, and 900 °C) provide insights into the TZM interactions and wear characteristics. As depicted in Fig. 8a, b, c, and d, these images reveal information regarding the pin's surface features and wear patterns. Firstly, the 3D profilometry images confirmed that the features observed on the

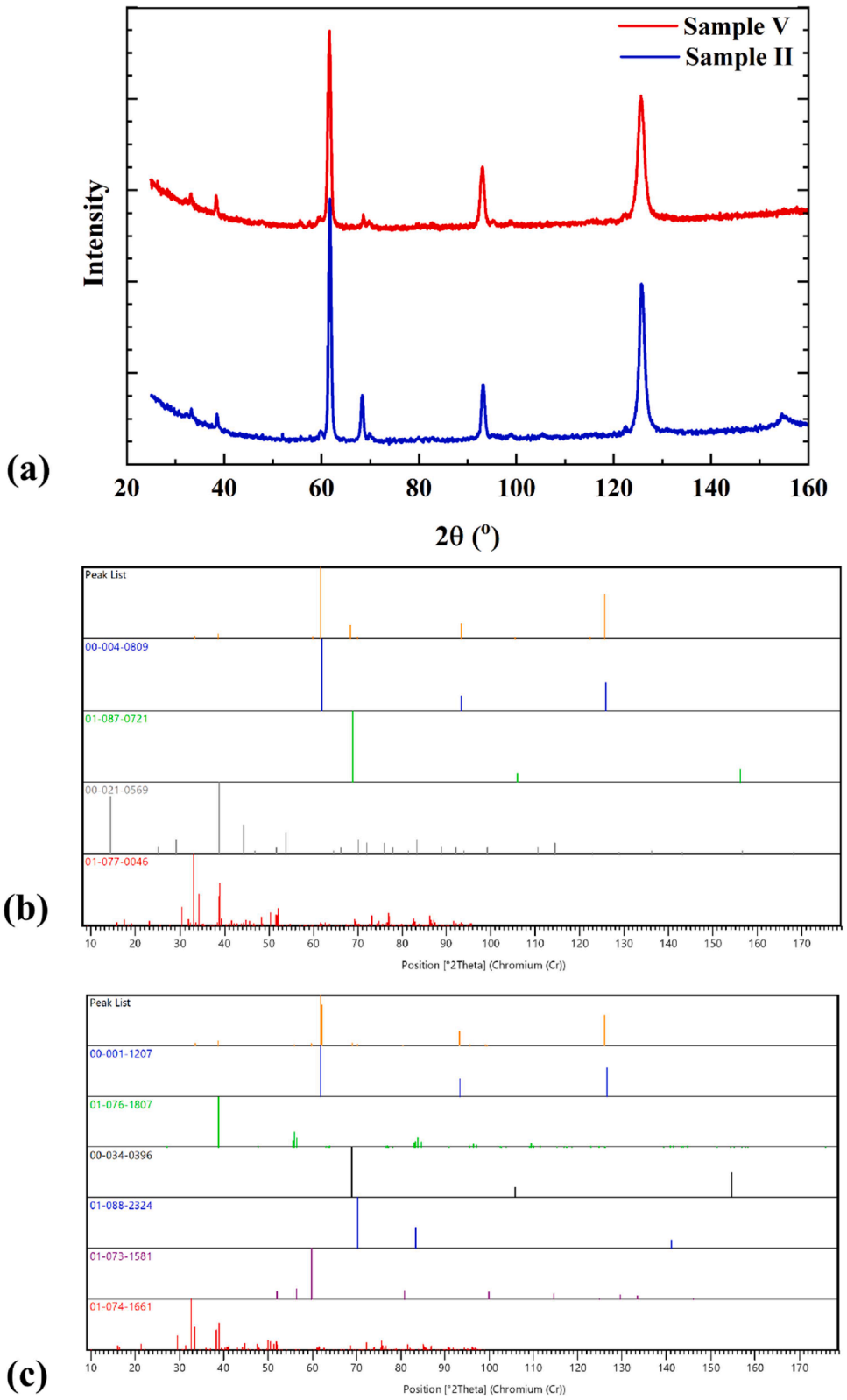

Fig. 11. (a) XRD results of Sample II and IV, plot of identified phases for (b) Sample II and (c) Sample IV.

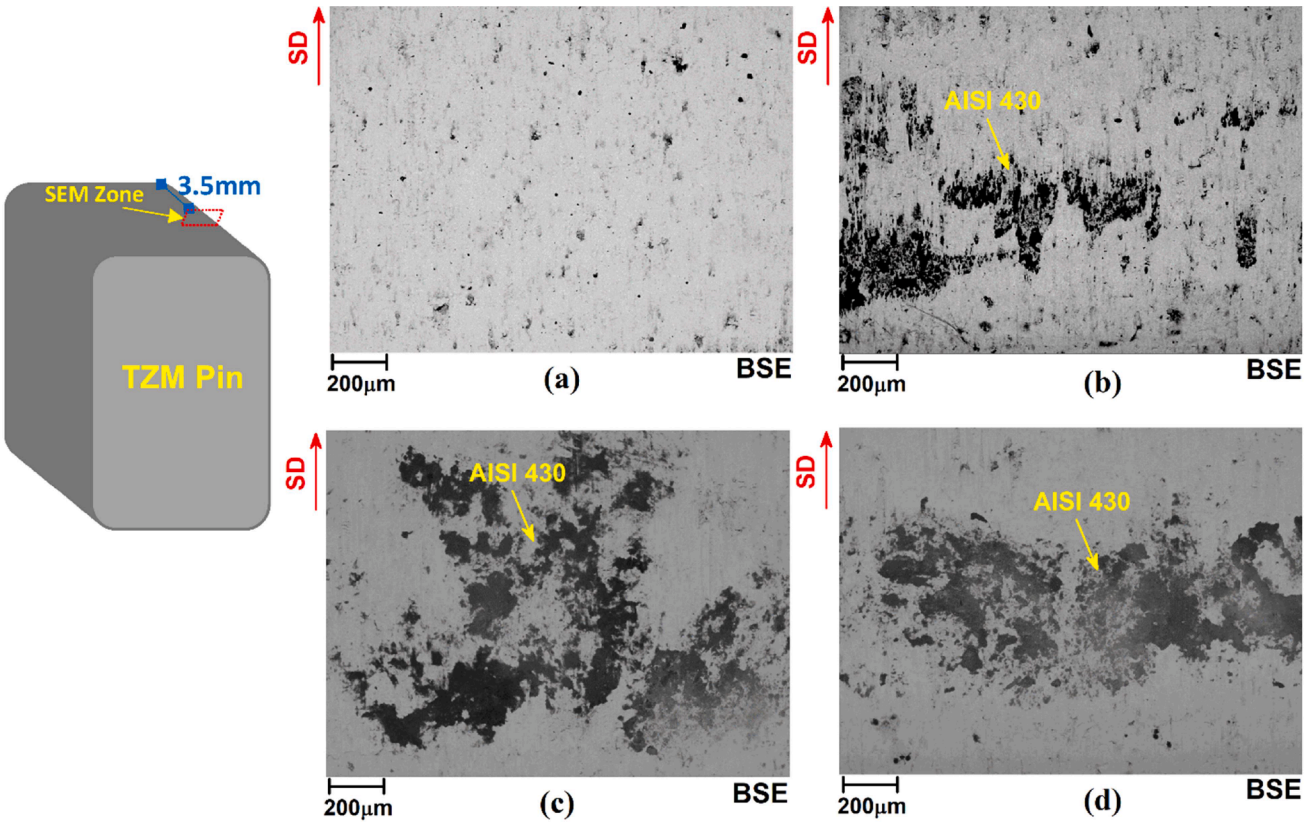

Fig. 12. SEM image from middle of (a) Sample I, (b) Sample II, (c) Sample III and (d) Sample IV pins.

right side of the pins, which correspond to the leading edge, were primarily the result of material galling and removal. This observation is evident in the images, where the undamaged TZM surface (as received) is characterized by lower topography, represented by shades of green (0μm), and a relatively flat surface. At a strip temperature of 25 °C, corresponding to room temperature, it is noteworthy that a smaller area of material removal occurred on the leading edge of TZM pin (as mentioned before).

This phenomenon can be attributed to several factors. One key factor is the lower reactivity of TZM and AISI 430 at room temperature [27]. This reduced reactivity results in decreased adhesion between the pin and the strip, coupled with the higher strength of the both pin and strip at room temperatures, which offers better resistance to wear [28]. However, as the AISI 430 steel strip temperature increases, there is a clear shift in the wear characteristics. Abrasive phenomena on the pin's surface become more pronounced and material adhesion at TZM pin increases. This is particularly evident in the 3D profilometry images, where the pin's surface exhibits a more significant adhesion, indicative of Galling. The most notable finding is the correlation between the strip temperature and the severity of adhesive wear.

As the strip temperature escalates to 900 °C, the 3D profilometry images clearly reveal a substantial increase in adhesive and abrasive wear on the TZM surface. This demonstrates that higher strip temperatures lead to more severe adhesive wear, emphasizing the importance of temperature in this frictional interaction. The roughness profiles of TZM samples with strips at 25 °C (Sample I) and 900 °C (Sample IV) are presented in Fig. 9a and b, respectively. The acquired results offer a detailed insight into the surface characteristics, revealing the presence of distinct wavy peaks in the roughness profiles that exhibit periodicity. In the case of Sample I, the roughness profiles display three prominent peaks, indicating a material transfer from AISI 430 steel to the TZM plug at 25 °C. As the strip temperature escalates, there is a noticeable directional shift in material transfer, with the transfer now occurring from the pin to the strip. The periodic peaks in Sample IV are more pronounced, showcasing a clear evolution in the material transfer dynamics. The adhesion periodic patterns, whether three at 25 °C or six at 900 °C, become increasingly conspicuous at higher temperatures, as depicted in Fig. 9a and b.

Despite variations in surface preparation patterning among samples, there is a consistent microscale trend in behavior across the tested pins. Both quantitative and qualitative insights emerge from the analysis, shedding light on the periodic deformation flow. Interestingly, the abrasive and adhesive wear on the TZM pin occurs in periodic cycles. Illustrated schematically in Fig. 9c, this flow outlines the formation of a jumping pattern (δ) on the surfaces of the AISI 430 strip and TZM pin after high-temperature testing. The emergence of this pattern appears to correlate with temperature-induced alterations in material transfer and adhesion patterns between the TZM pin and AISI 430 strip surfaces.

The average Sa and Sq of surfaces are collected and presented in Fig. 10a and b, respectively. The average Sa for Sample I, II, III, and IV were 2.2 μm, 3.1 μm, 3.8 μm and 4 .3μm. The results revealed the average Sq for Sample I, II, III, and IV were 4.6 μm, 5.7 μm, 6.5 μm and 7.6 μm, respectively. The Sa values for all samples are notably higher than those of the raw pin. This indicates that the surface of the TZM pins experienced increased roughness after the friction tests. The increase in Sa suggests material removal and adhesive wear during the tests, which is consistent with the observations from the 3D profilometry images discussed earlier.

As the strip temperature increases, there is a consistent trend of increased Sa values, with Sample IV (tested at 900 °C) having the highest Sa. This increase in Sa suggests that the more adhesive wear on the pin's surface becomes more severe at higher temperatures. The Sa values follow a decreasing trend, indicating that surface wear is less prominent at lower strip temperatures, presumably due to material reactivity and strength differences. Similar to Sa, the Sq values for all samples are higher than that of the raw pin, reinforcing the notion of increased

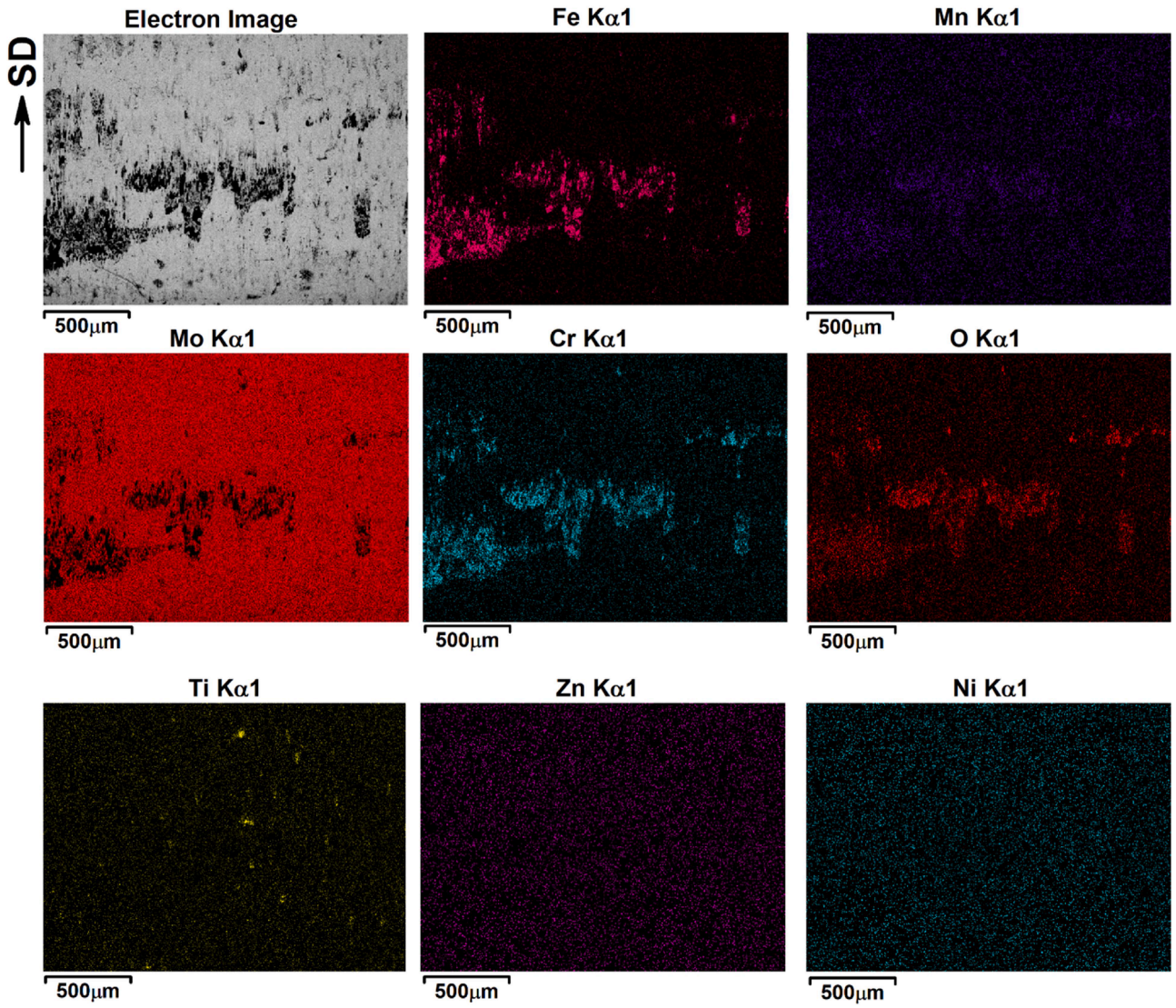

Fig. 13. EDS element maps of Sample II.

roughness due to the friction tests. The Sq values also exhibit an increasing trend with increasing strip temperature. Sample IV (900 °C) shows the highest Sq, indicating a rougher surface than the other samples. The decreasing Sq values suggest that while the overall roughness is reduced at lower strip temperatures, the wear pattern remains consistent with the Sa results. The percentage change in Sa and Sq values provides a clearer perspective on the extent of surface roughness alteration due to the friction tests. Sample IV (900 °C) experienced the most significant percentage increase in both Sa and Sq, with Sa increasing by approximately 168.75 % and Sq increasing by around 216.67 % (Compared to raw TZM). As the AISI 430 strip temperature decreased, the percentage change in both Sa and Sq decreased, indicating a reduction in abrasive wear.

For Sample I (25 °C), Sa and Sq increased by only about 37.5 % and 91.67 %, respectively, indicating the least abrasive wear among the tested samples. The data analysis reveals important insights into the impact of strip temperature on the wear characteristics of TZM pins. As the temperature increases from 25 °C to 900 °C, a consistent trend of increased surface roughness (Sa and Sq) observed. This suggests that higher strip temperatures lead to more severe abrasive and adhesive wear on the TZM pins (As seen in surface topography). One plausible explanation for this phenomenon is the influence of temperature on material reactivity and adhesion. The adhesion between the TZM pins and the AISI 430 strip is stronger at higher temperatures, resulting in more significant material removal and higher surface roughness. However, at lower strip temperatures, the reactivity between the materials decreases, reducing adhesion and, subsequently, more abrasive wear. This interpretation aligns with the earlier findings from the 3D profilometry images, which indicated that adhesive wear became more severe as the strip temperature increased. The Sa and Sq values provide quantitative support for these visual observations. They confirm that the TZM pins' surfaces are subject to increasing wear and roughening as the strip temperature rises. Comparing the results of the samples with the raw pin data further underscores the impact of the friction tests. Both Sa and Sq values for the raw pin are significantly lower than those for the tested samples, emphasizing the substantial material removal and surface roughening due to the tests.

3.4. XRD results

The XRD results for Sample II and Sample IV are presented in Fig. 11a, while detailed phase plots for Sample III and Sample V are shown in Figs. 11b and c, respectively. The XRD results for Sample I predominantly show the components of the parent materials. In contrast, the XRD analysis of Sample II reveals the presence of Mo, Fe, MoO_3, and Mo_9O_{26} phases on its surface. As expected, the TZM alloy's

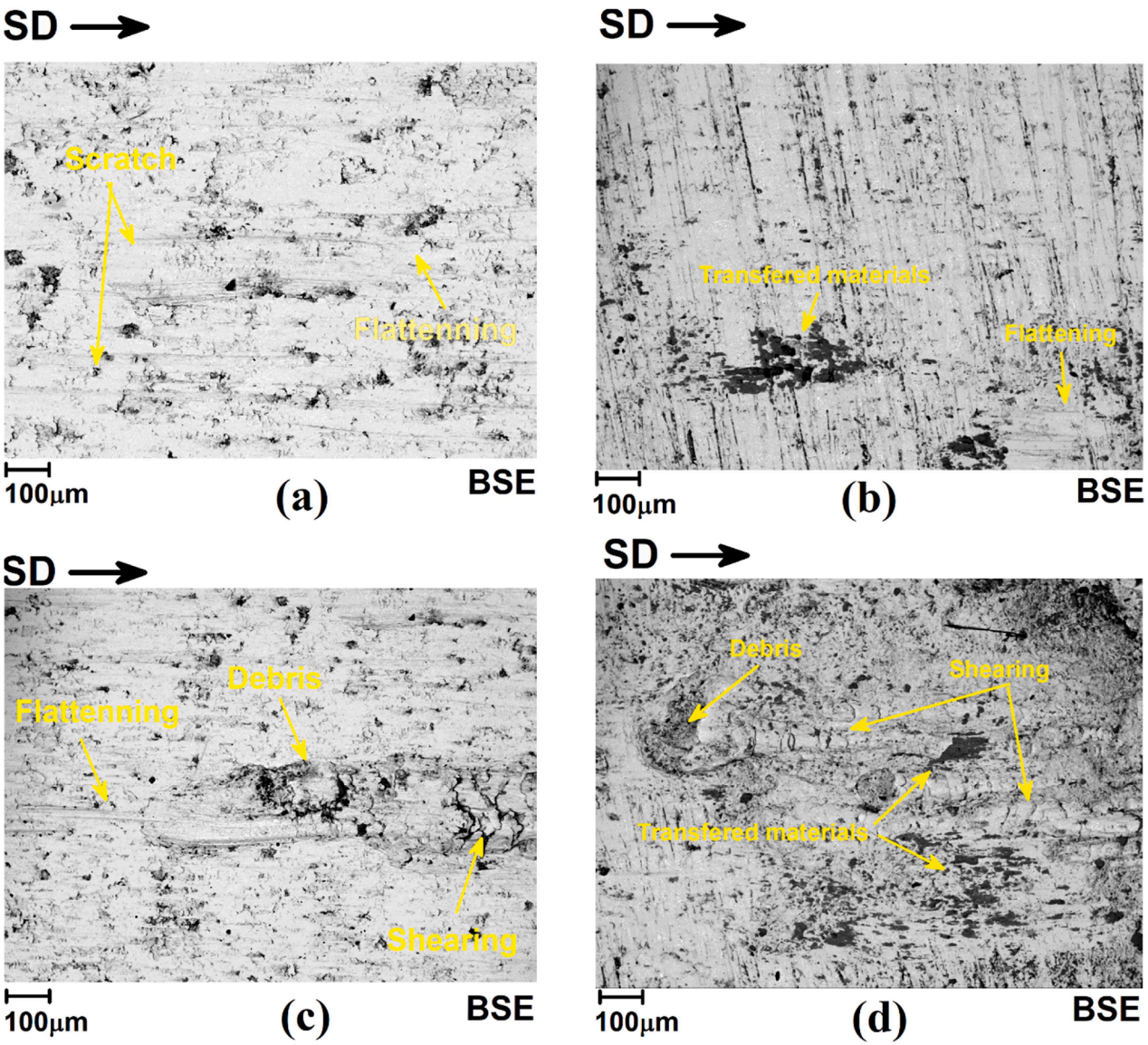

Fig. 14. SEM image from wear of (a) Sample I, (b) Sample II, (c) Sample III and (d) Sample IV pins.

primary constituent, molybdenum, is observed. However, the detection of Fe, which is absent in the TZM composition, likely originates from the AISI 430 steel strip material, suggesting surface transfer to the pin after testing. The oxide phases present are likely derived from the steel strip, which was preheated to 300 °C before testing, increasing the likelihood of oxide formation on its surface. The tribometer setup may have contributed to the initial oxide presence on the TZM pin, as the pressure applied during testing could promote oxide adhesion. Additionally, during pin sliding, debris formation may have resulted in further bonding on the TZM surface. MoO_3 contains molybdenum in $a + 6$ oxidation state combined with oxygen, while Mo_9O_{26} has a more complex stoichiometry with mixed oxidation states, typically a combination of +6 and lower states. This compound also features a more intricate crystal structure, often composed of both MoO_6 octahedra and MoO_4 tetrahedra, creating a complex arrangement [29]. The detection of these oxides suggests substantial interaction at the contact interface between the TZM alloy and the steel during tribotesting. Elevated temperatures and friction likely facilitate the oxidation of molybdenum on Sample II. The presence of MoO_3 and Mo_9O_{26} phases could enhance the oxidation and wear resistance of both the TZM alloy and the steel counterface by reducing direct contact and mitigating severe wear. The XRD results for Sample IV indicate the presence of Mo, Fe, MoO_2, Mo_8O_{23}, TiO_2, and Fe-Cr phases on the surface. During the high-temperature tribotest (900 °C on the steel strip), heat transfer between the pin and strip likely led to increased local temperatures and potentially limited oxygen availability, favoring the formation of molybdenum in lower oxidation states, such as MoO_2, which has $a + 4$ oxidation state. MoO_2 forms under more reducing conditions than MoO_3, suggesting areas within the contact interface experience localized oxygen depletion and high temperatures. The presence of TiO_2 indicates oxidation of the titanium component within the TZM alloy, contributing to the overall oxide layer on the surface.

Under normal loading, sliding velocity, and high temperatures, complex, non-stoichiometric molybdenum oxides like Mo_8O_{23} can form due to varying oxidation environments and localized temperature gradients. Mo_8O_{23}, containing molybdenum in mixed oxidation states, suggests the presence of both reducing and oxidizing conditions at the interface during testing. The detection of Fe-Cr phases indicates substantial interaction between the steel counterface and the TZM alloy, likely forming a mixed layer or tribofilm incorporating elements from both materials. The increased softening of the steel counterface at 900 °C promotes material transfer to the TZM surface, leading to Fe-Cr deposition and the formation of a tribofilm that integrates components

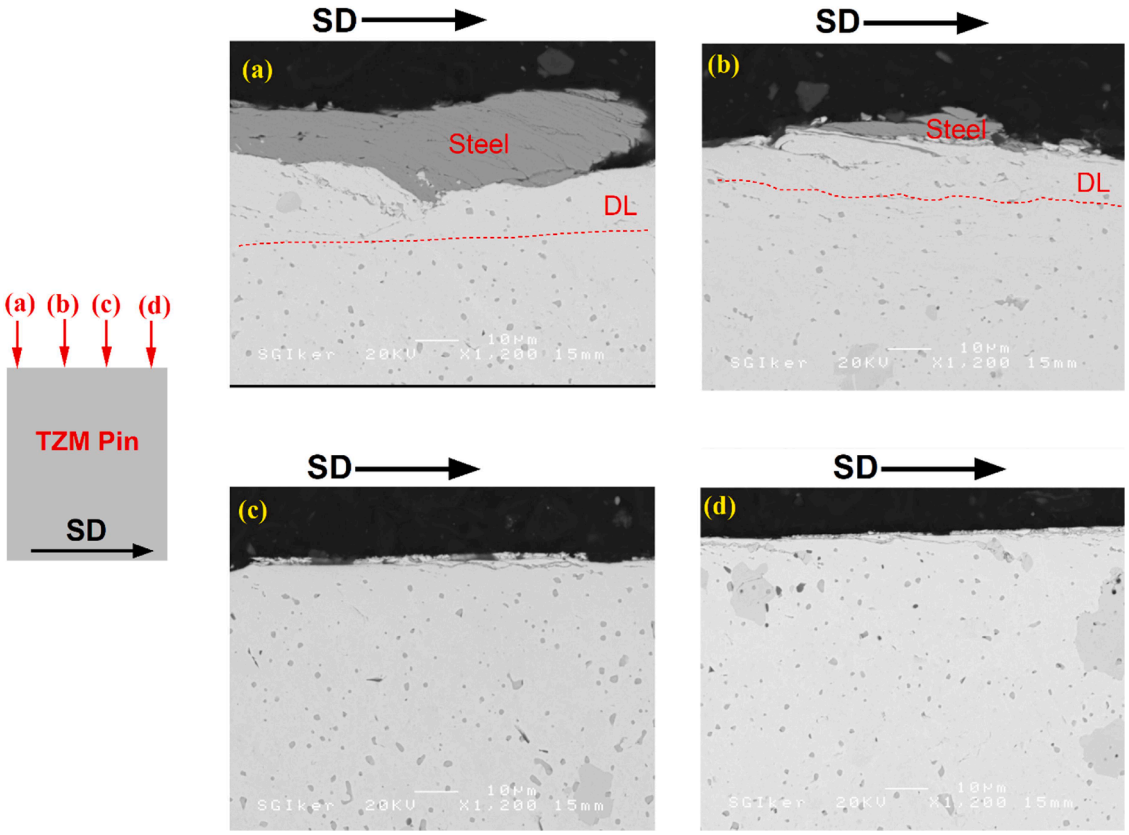

Fig. 15. Cross section view SEM image from wear Sample II.

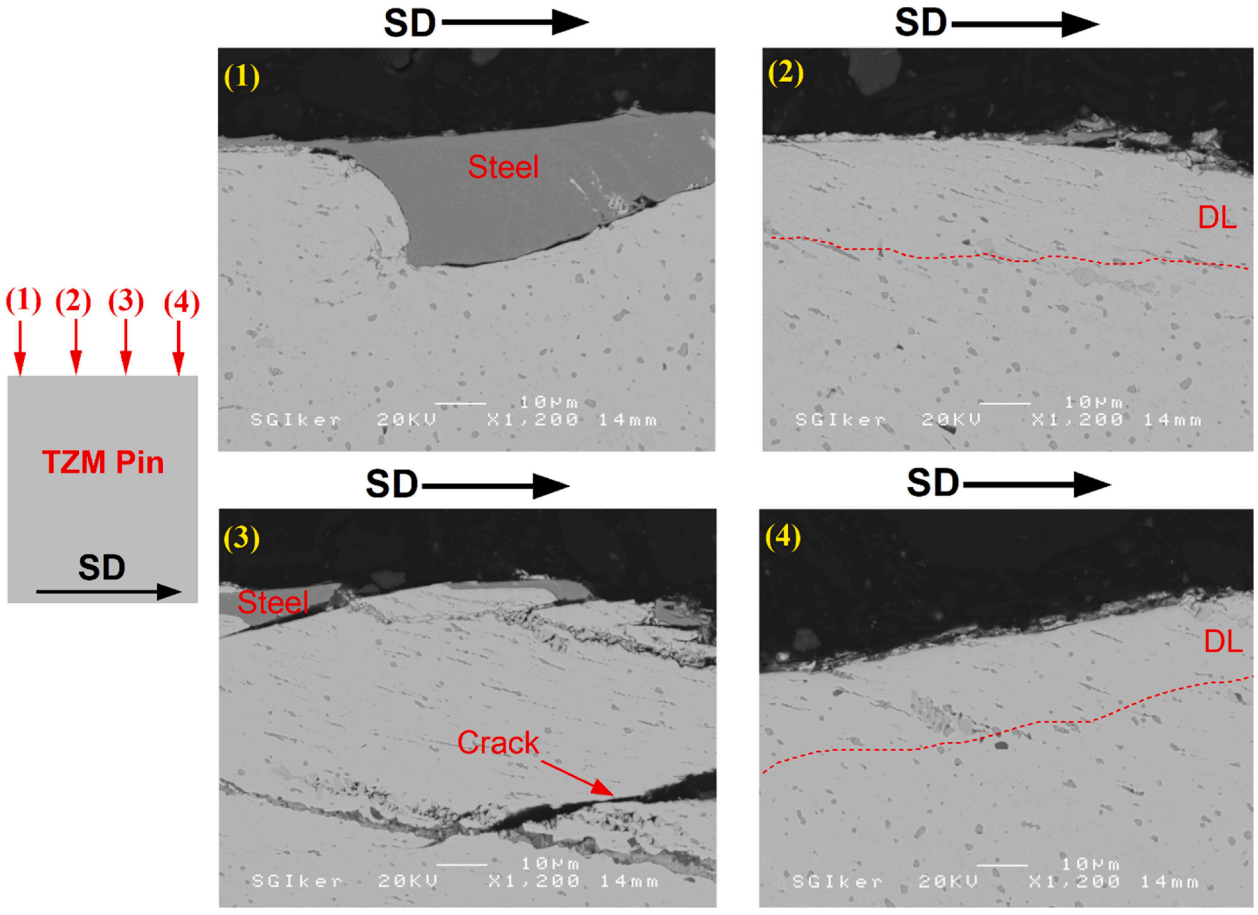

Fig. 16. Cross section view SEM image from wear Sample IV.

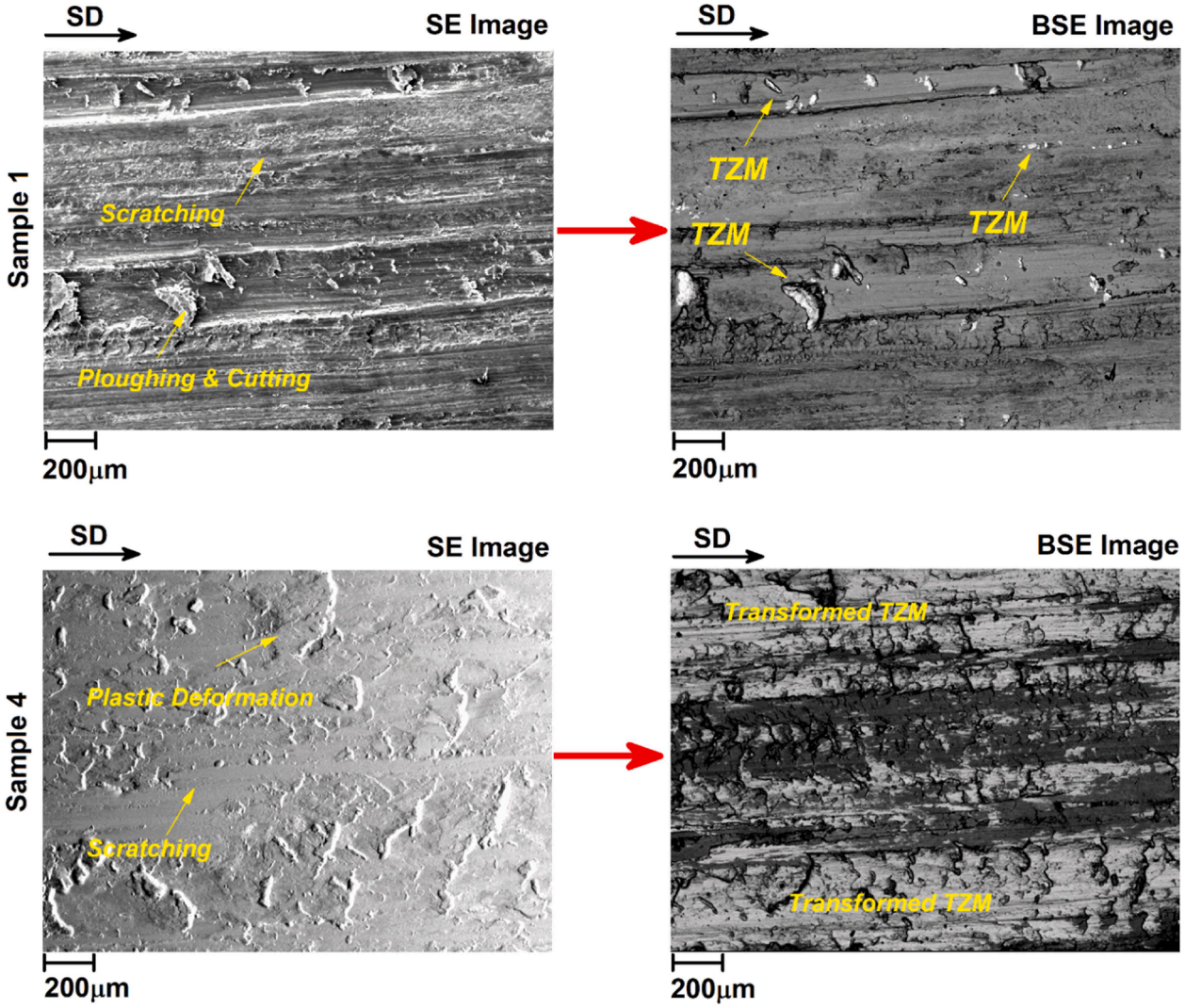

Fig. 17. SEM image from surface of AISI 430 steel strip that tested with Sample I and Sample IV.

from both the steel and TZM alloy.

3.5. Wear mechanism

The SEM image analysis was carried out from the middle of the pins after tests with low magnifications. The SEM analysis from the middle of the pins at low magnifications provides a macroscopic perspective, shedding light on the overall wear behavior. Fig. 12a, b, c, and d present the results of Samples I, II, III, and IV, respectively. The results show on the surface of Sample I small pieces of AISI 430 steel (black dots) staked on the surface of pin without significant damage suggests a relatively mild wear mechanism. In this case, temperature does not significantly affect material transfer between TZM pin and steel strip. Significant damage was not detected on the pin surface, and it shows the pin had enough strength during the sliding encounter of the strip. The lack of substantial damage on the pin surface indicates that the pin possesses sufficient strength to withstand the sliding encounters with the strip at these lower temperatures. This point can be expected because the hardness and tensile strength of TZM are more than AISI 430 steel at room temperature (as mentioned in Tables 1 and 2).

As the AISI 430 steel strip temperature increases, the emergence of dark zones on the pin surface becomes apparent, indicating a shift in the wear mechanism. The dark zones are identified as steel strip material bonded to the pin surface, implying a more significant role of temperature in the wear process. This transition could be attributed to changes in the material properties at elevated temperatures, leading to enhanced adhesion or other wear mechanisms. As an example, an EDS map from sample II is presented in Fig. 13. The EDS map further supports this observation by revealing that the dark zones consist of elements from the AISI 430 strip material. The temperature-dependent adhesive wear mechanism elucidated in these results emphasizes the importance of considering thermal effects in understanding and mitigating wear in these tribotests.

The high magnification SEM images from the surface of Samples I, II, III, and IV are presented in Figs. 14a, b, c and d, respectively. The results show that at room temperature (Fig. 14a), scratch and flattening are the predominant wear mechanisms observed. The low material transfer and absence of surface damage suggest that the contact conditions at interface was are not severe comparing to heated strip condition. The hardness of the pin (220HV) is higher than that of the strip (162HV), indicating that the pin is harder and less prone to wear. The relatively low-test temperature further supports abrasive wear, as the mechanical properties of both materials are not significantly affected [30]. At an elevated temperature of 300 °C (Fig. 14b), the wear mechanism remains scratchy and flattening, but there is a slight increase in material transfer locally. The higher temperature likely induces thermal softening in the TZM pin and AISI 430 strip materials [27]. This softening could facilitate material transfer between the pin and strip, leading to the observed local

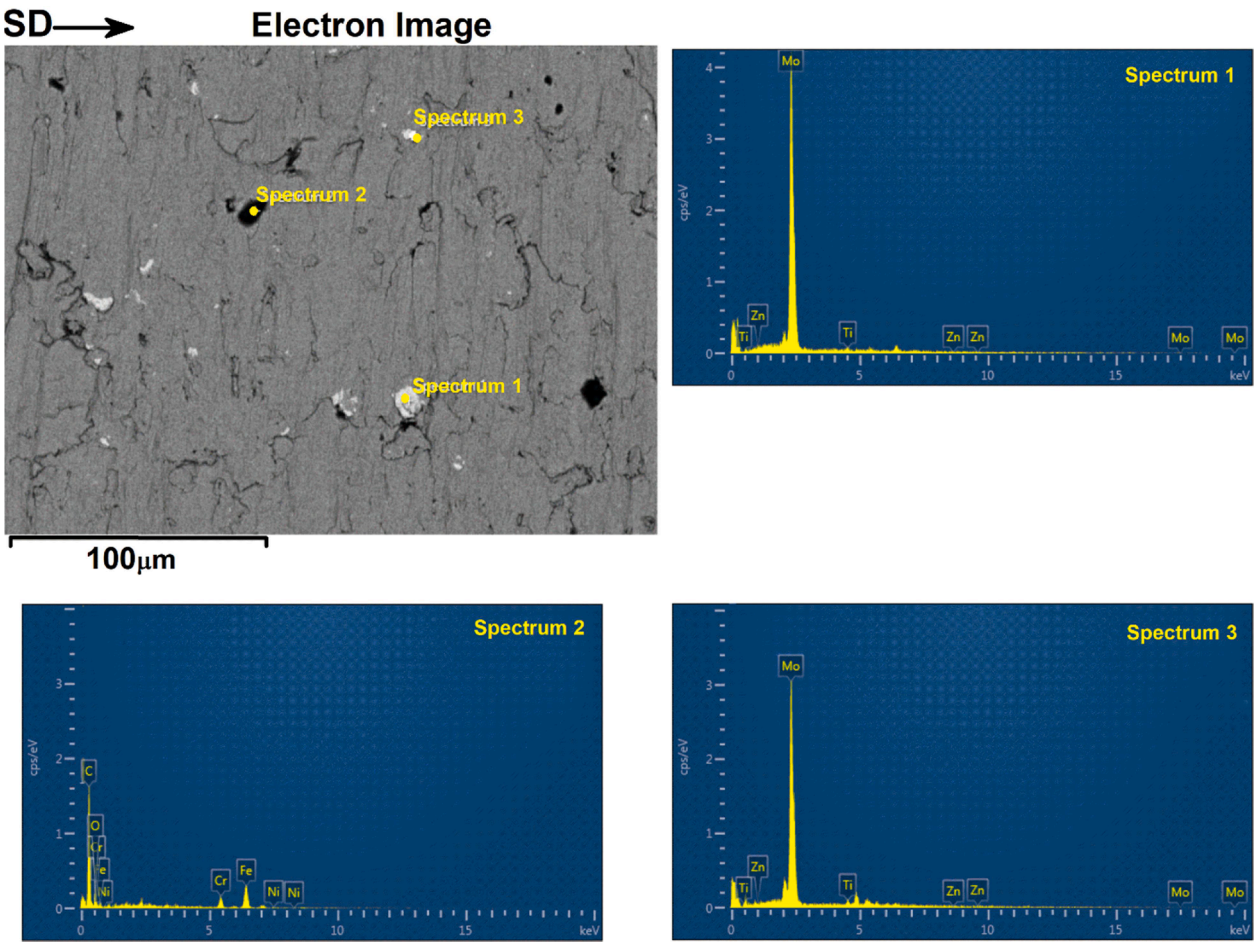

Fig. 18. SEM image from surface of AISI 430 steel strip that tested with Sample I with DES point analysis results.

adhesive wear. The extent of wear is still relatively low due to the moderate temperature. At 600 °C (Fig. 14c), the wear mechanism continues to be scratch and flattening, but additional observations include agglomerated wear debris and surface shearing. The elevated temperature has a more pronounced effect on material properties, potentially causing increased plastic deformation and more adhesion between the TZM pin and the AISI 430 strip. The agglomerated wear debris and surface shearing suggest more severe wear conditions and enhanced interaction between the pin and strip materials.

At 900 °C (Sample IV), the wear mechanism significantly changes comparing to other cases. The SEM image from surface of Sample IV is present in Fig. 14d. There is a high material transfer between the TZM pin and AISI 430 strip, increased shearing bonds, and agglomerated wear debris. The elevated temperature has likely led to significant softening of both materials, promoting more intense adhesion and material transfer. The observed shearing bonds and agglomerated wear debris indicate a more severe wear condition. These results support the jumping pattern idea presented in Fig. 9. The temperature notably impacts the wear mechanisms observed in the tribometer tests. As the temperature increases, the TZM becomes more susceptible to wear due to thermal softening, which promotes adhesion and material transfer. The progression from scratch and flattening to agglomerated wear debris and increased shearing bonds reflects the temperature-induced changes in the mechanical properties of the TZM pin and AISI 430 steel strip materials.

The cross-sectional SEM image of different areas of Sample II is presented in Fig. 15. This image reveals internal defects in the TZM pin at the surface level. Points (1), (2), (3), and (4) correspond to the leading, middle, and back sides of the TZM pin. The results show visible adhesion of steel at the pin's tip. Additionally, a deformation layer (DL) has formed just below the surface, a result of the thermo-mechanical interaction between the pin and the strip during the tribotest. The DL is thicker at the tip of the pin compared to the middle region. Small cracks are also observed on the surface of the TZM pin after tribo test. The cross-sectional SEM image further reveals that some surface defects are deeper than what is visible in the surface-level SEM image.

As the contact temperature increases (with the strip reaching 900 °C), both the pin and strip soften, leading to an increase in the thickness of the deformation layer (DL). Additionally, surface cracking on the pin intensifies, as shown in Fig. 16. The thicker DL layer is formed in all areas (from point (1) to point (4)). In this case, a mechanically mixed layer can be detected at center of TZM pin. A big crack separated DL and mixture layer from TZM matrix.

The SE and BSE images of strips for tribotest I and IV are presented in Fig. 17. The results obtained show that at the low temperature of 25 °C, scratching, ploughing, and cutting phenomena align with expectations. This AISI 430 steel behavior at 25 °C indicates that the TZM pin's higher hardness and superior mechanical properties enable it to deform the AISI 430 steel strip easily. This is a typical response in such tests, where a more robust tool material interacts with a deformable body. The presence of small points of pin material on the surface of the 25 °C strip suggests that the interaction between the TZM pin and the AISI 430 steel strip was minimal at this temperature, likely due to the relatively lower deformation forces exerted by the pin on the steel.

As the strip temperature increased to 900 °C, the SEM image analysis indicated a shift in the deformation behavior. With the reduction in mechanical properties of both the AISI 430 steel strip and the TZM pin at higher temperatures, there is an observed increase in strip deformation,

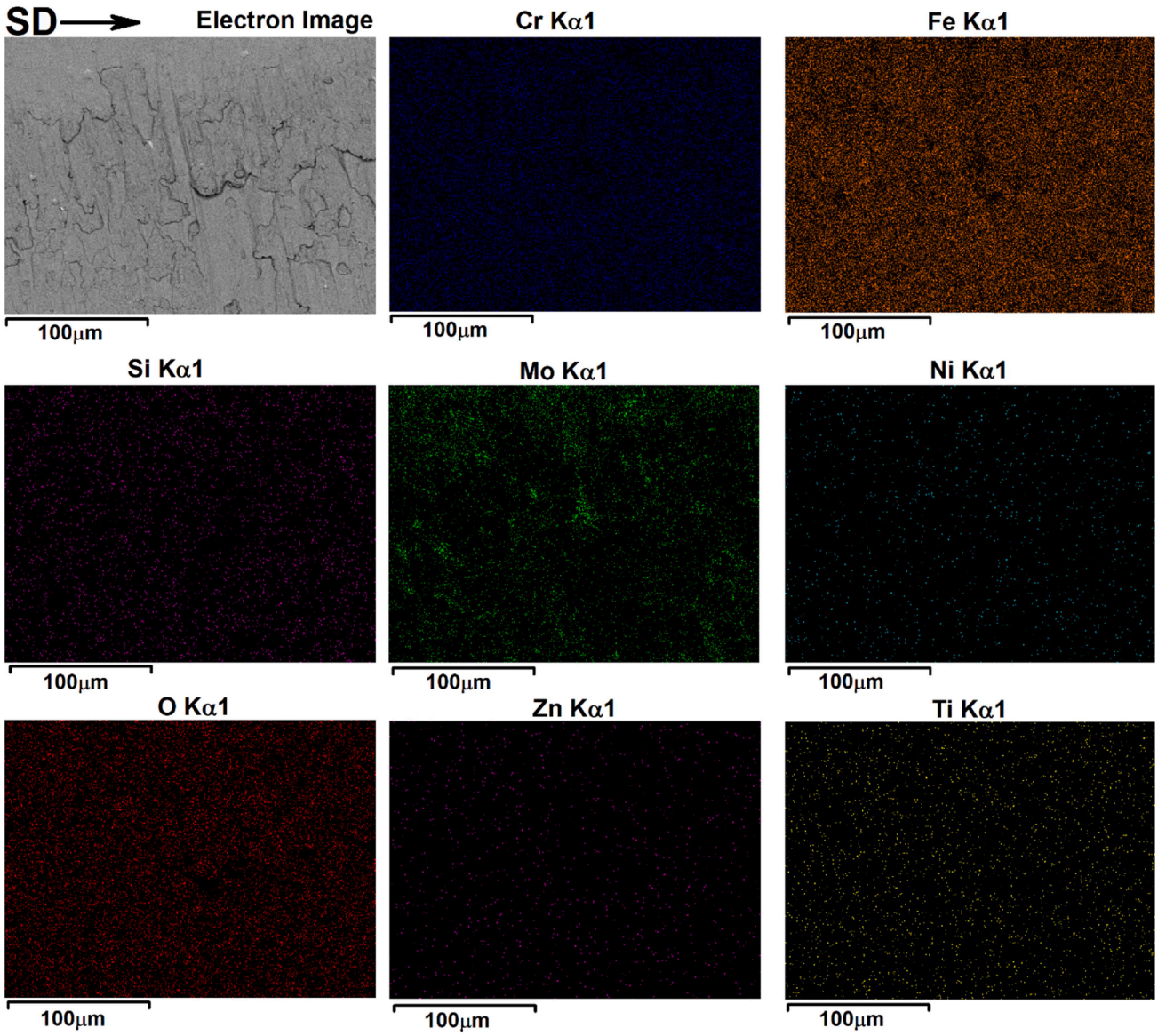

Fig. 19. EDS elements map from transferred layer area at Sample IV.

characterized by flattening and scratching. This aligns with the expected trend, as elevated temperatures generally lead to decreased material strength and increased ductility. Interestingly, the transformed layer of TZM material on the AISI 430 steel strip becomes more apparent at higher temperatures, reflecting the changing nature of the interaction between the pin and the strip. The enhanced deformation and the visible transformation layer underscore the intricate relationship between temperature, material properties, and the resulting deformation processes. The high-magnification SEM image from Sample I is depicted in Fig. 18. The EDS point analysis was carried out with the point on the surface of the strip. The EDS results exposed that these points are from pin material.

The EDS map analysis from the transferred layer on Sample IV is presented in Fig. 19. The EDS map analysis specifically focused on the transformed layer, revealing the distribution of TZM material on the surface of the AISI 430 steel strip. As can be seen, the EDS element detected the distribution of both TZM and AISI 430 steel materials in the analyzed area.

The results show the non-uniform distribution of TZM on the surface of the strip because the concentration of TZM elements (Mo, Ti, and Zn) was higher at some points. The non-uniform distribution may indicate localized variations in temperature, pressure, or other dynamic parameters during the friction test. The presence of TZM elements on the AISI 430 steel strip surface and the observed thin thickness of the remaining TZM pin material indicates that a significant transformation or transfer of material occurred during the 900 °C strip temperature. As can be seen, the TZM elements are detected on the AISI 430 strip surface with various concentrations (based on the EDS map of Mo, Zn, and Ti), suggesting that material transfer or adhesion occurred. Still, it was not uniform across the entire surface. This phenomenon may be attributed to localized variations in contact pressure or temperature gradients during the friction test.

4. Conclusions

This investigation delves into the influence of AISI 430 steel strip temperature on the friction and wear mechanisms of TZM. Varied strip temperatures, spanning 25 °C, 300 °C, 600 °C, and 900 °C, correspondingly led to contact temperatures of 25 °C, 110 °C, 195 °C, and 300 °C. The following key conclusions emerge from our findings:

1. The coefficient of friction (COF) between TZM and AISI 430 demonstrates a consistent decrease with rising contact temperatures. Specifically, the COF reduced by 11.5 %, transitioning from 0.77 at 25 °C to 0.69 at 900 °C for both pin and strip interfaces.
2. An intriguing jumping pattern manifested on the strip's surface as the test temperature exceeded room temperature. The distance of this pattern decreased proportionally with the elevated testing temperature, suggesting a concurrent interplay of adhesion and deformation between TZM and AISI 430 steel, with the deformation serving as the root cause.
3. The TZM pin, subjected to a 900 °C strip, exhibited a noteworthy percentage increase in both Sa (168.75 %) and Sq (216.67 %), compared to the raw TZM. This surge indicates heightened abrasive wear at elevated temperatures, attributed to strengthened adhesion and substantial material removal between TZM pins and the AISI 430 strip.
4. At 25 °C contact temperature, scratch and flattening emerged as predominant wear mechanisms, signifying less severe contact conditions. Conversely, as the strip temperature escalated to 900 °C (resulting in a 300 °C contact temperature), the wear mechanism shifted to shearing, accompanied by increased material transfer from AISI 430 steel to TZM. Notably, TZM particles adhered to the AISI 430 steel surface, transforming into a discernible TZM layer with temperature elevation. These nuanced observations contribute to a comprehensive understanding of the intricate dynamics governing TZM behavior under varying temperature conditions.

CRediT authorship contribution statement

Hamed Aghajani Derazkola: Writing – original draft, Visualization, Validation, Resources, Methodology, Investigation, Formal analysis, Conceptualization. **Leonardo Pelcastre:** Validation, Supervision, Software, Methodology. **Eduardo Garcia:** Writing – original draft. **Pello Jimbert:** Validation, Methodology, Investigation. **Jens hardell:** Writing – original draft, Validation, Supervision.

Declaration of competing interest

The authors declare that they have no known competing financial interests or personal relationships that could have appeared to influence the work reported in this paper.

Acknowledgements

The authors thank for technical and human support provided by SGIker (UPV/EHU/ ERDF, EU).

Data availability

Data will be made available on request.

References

[1] H. Sirali, D. Simsek, D. Ozyurek, Investigation of the effect of zirconium amount on grain size and wear performance in TZM alloys produced by mechanical alloying method, Trans. Ind. Instit. Metals 75 (2022) 805–812, https://doi.org/10.1007/s12666-021-02510-4.

[2] K. Surani, S. Patel, A.J. Alrubaie, A. Oza, H. Panchal, S. Kumar, S. Zahmatkesh, Performance comparison of powder mixed EDM and traditional EDM on TZM-molybdenum super alloy using response surface methodology, Int. J. Interact. Des. Manuf. (2022), https://doi.org/10.1007/s12008-022-01088-5.

[3] B. Tuncay, D. Ozyurek, Effects of titanium addition on the microstructure and electrochemical corrosion behaviour in TZM alloy, Appl. Phys. A 128 (2022) 746, https://doi.org/10.1007/s00339-022-05867-5.

[4] K. Surani, S. Patel, H. Panchal, N. Gupta, T. Shinde, Y. Sharma, Mathematical modeling for radial overcut on powder mixed micro-electrical discharge machining (μ-EDM) of TZM-molybdenum superalloy by response surface methodology, Int. J. Interact. Des. Manuf. (IJIDeM) (2023), https://doi.org/10.1007/s12008-023-01443-0.

[5] S.P. Chakraborty, S. Banerjee, K. Singh, I.G. Sharma, A.K. Grover, A.K. Suri, Studies on the development of protective coating on TZM alloy and its subsequent characterization, J. Mater. Process. Technol. 207 (2008) 240–247, https://doi.org/10.1016/j.jmatprotec.2007.12.075.

[6] H. Sıralı, D. Şimşek, D. Özyürek, Effect of Ti content on microstructure and wear performance of TZM alloys produced by mechanical alloying method, Met. Mater. Int. 27 (2021) 4110–4119, https://doi.org/10.1007/s12540-020-00735-4.

[7] H. Wang, H. Ren, L. Qiu, H. Jiang, Z. Gao, X. Hu, X. Pan, M. Zhu, Y. Zhang, Effect of Al content on 1200 °C steam oxidation behavior of Cr-based coatings on TZM alloy, Corros. Sci. 219 (2023) 111239, https://doi.org/10.1016/j.corsci.2023.111239.

[8] Z. Zhang, X. Li, E. Almandoz, G.G. Fuentes, H. Dong, Sliding friction and wear behaviour of titanium-zirconium-molybdenum (TZM) alloy against Al2O3 and Si3N4 balls under several environments and temperatures, Tribol. Int. 110 (2017) 348–357, https://doi.org/10.1016/j.triboint.2016.10.049.

[9] J.A. Schey, Material aspects of friction and wear in manufacturing processes, JOM 32 (1980) 28–33, https://doi.org/10.1007/BF03354541.

[10] L. Gu, Y. Zhu, F. Zhang, A. Farhadi, W. Zhao, Mechanism analysation and parameter optimisation of electro discharge machining of titanium-zirconium-molybdenum alloy, J. Manuf. Process. 32 (2018) 773–781, https://doi.org/10.1016/j.jmapro.2018.03.002.

[11] T. Liu, P. Hu, S.-L. Li, Q.-S. Shi, R. Bai, B. Jin, B.-L. Hu, X. Wang, Li-Wang, J.-Z.; Yang, et al., Oxygen content effect on mechanical properties and microstructure of TZM alloy, Mater. Charact. 203 (2023) 113075, https://doi.org/10.1016/j.matchar.2023.113075.

[12] H. Zhou, Y. Zhang, X. Hua, Z. Yang, High-temperature anti-wear behavior of alumina-reinforced Ti–Zr–Mo alloy composites, Wear. 319 (2014) 184–190, https://doi.org/10.1016/j.wear.2014.08.003.

[13] E. Kalns, Effects of surface hardening treatments on wear resistance of Mo and TZM sheet, JOM 29 (1977) 7–11, https://doi.org/10.1007/BF03354313.

[14] B. Tian, R. Zhu, Y. Zhou, G. Wei, K. Dong, A static balance model and analysis of 430 stainless steel produced by basic oxygen furnace–Argon oxygen decarburization furnace process, Steel. Res. Int. 93 (2022) 2100852, https://doi.org/10.1002/srin.202100852.

[15] R. Iquilio Abarzúa, E. Hernández-Durán, T. Nguyen-Minh, L.A.I. Kestens, J.L. Valín Rivera, Castro Cerda, F.M. Microstructure, Anisotropy and formability evolution of an annealed AISI 430 stainless steel sheet, Steel. Res. Int. 93 (2022) 2100114, https://doi.org/10.1002/srin.202100114.

[16] M. Sun, S. Liu, Y. Cheng, Z. Cheng, R. Ren, C. Chen, Microstructure characteristics and mechanical properties of the thin-plate AISI 430 ferritic stainless steel joints by interrupted pulsed arc welding, J. Mater. Res. Technol. 21 (2022) 4500–4511, https://doi.org/10.1016/j.jmrt.2022.11.063.

[17] W. Lopes, E.C.S. Corrêa, H.B. Campos, M.T.P. Aguilar, P.R. Cetlin, Effect of reverse and cyclic shear on the work-hardening of AISI 430 stainless steel, J. Mater. Sci. 44 (2009) 441–448, https://doi.org/10.1007/s10853-008-3121-0.

[18] V.D. Luiz, P.C. de Matos Rodrigues, Failure analysis of AISI 430 stainless steel sheet under stretching and bending conditions, Int. J. Adv. Manuf. Technol. 121 (2022) 2759–2772, https://doi.org/10.1007/s00170-022-09451-2.

[19] N. Senthilkumar, G. Perumal, K. Palanikumar, B. Deepanraj, M.S. Basha, Wear and mechanical characteristics of coated Ti-6Al-4 V alloy with an alumina-13 wt.% titania -40 wt.% yitrium stabilized zirconia ceramic composite via plasma spraying technique, Results. Eng. 25 (2025) 103777, https://doi.org/10.1016/j.rineng.2024.103777.

[20] X. Li, H. Li, Q. Li, C. Jin, K. Hua, H. Wang, The determining role of Al addition on tribology properties and oxidation behavior at elevated temperatures of TiZrHfNb refractory high-entropy alloy, Mater. Charact. 189 (2022) 111921, https://doi.org/10.1016/j.matchar.2022.111921.

[21] X. Li, C. Jin, H. Li, X. Hao, K. Hua, X. Deng, H. Wang, Z. Wang, A combinatorial assessment of microstructure and mechanical properties in AlCrCuFeNi2Vx concentrated alloys, J. Alloys. Compd. 906 (2022) 164304, https://doi.org/10.1016/j.jallcom.2022.164304.

[22] M. Sana, M.U. Farooq, S. Hassan, A. Khan, On the machine learning algorithm combined evolutionary optimization to understand different tool designs' Wear mechanisms and other machinability metrics during dry turning of D2 steel, Results. Eng. (2025) 103998, https://doi.org/10.1016/j.rineng.2025.103998.

[23] B. Fischer, M. Beschliesser, A. Hoffmann, S. Vorberg, Mechanical properties of refractory metals at extremely high temperatures, Mater. Sci. Forum 534–536 (2007) 1269–1272, https://doi.org/10.4028/www.scientific.net/MSF.534-536.1269.

[24] A. Rassili, Modelling and experimental investgations of tooling issues for thixoforming of steel, Solid State Phenomena 285 (2019) 347–353, https://doi.org/10.4028/www.scientific.net/SSP.285.347.

[25] G. Filacchioni, E. Casagrande, U. De Angelis, G. De Santis, D. Ferrara, Tensile and impact properties of TZM and Mo-5% re, J. Nucl. Mater. 212–215 (1994) 1288–1291, https://doi.org/10.1016/0022-3115(94)91037-5.

[26] L. Deng, L. Pelcastre, J. Hardell, B. Prakash, M. Oldenburg, Experimental evaluation of galling under press hardening conditions, Tribol. Lett. 66 (2018) 93, https://doi.org/10.1007/s11249-018-1023-0.
[27] T. Mrotzek, A. Hoffmann, U. Martin, H. Oettel, Evolution of microstructure during hot deformation of the PM Molybdenum alloy TZM, Mater. Sci. Forum 539–543 (2007) 2725–2730, https://doi.org/10.4028/www.scientific.net/MSF.539-543.2725.
[28] R.P. Walters, B.S. Covino, Evaluation of high-temperature diffusion barriers for the Pt-Mo system, Metallurg. Trans. A 19 (1988) 2163–2170, https://doi.org/10.1007/BF02645041.
[29] S. Dong, W. Cheng, J. Yao, Influence of reciprocating friction on friction and wear characteristics of MoS2 films, Results. Eng. 18 (2023) 101073, https://doi.org/10.1016/j.rineng.2023.101073.
[30] T. Mrotzek, U. Martin, A. Hoffmann, High temperature deformation behavior of the molybdenum alloy TZM, J. Phys. Conf. Ser. 240 (2010) 012079, https://doi.org/10.1088/1742-6596/240/1/012079.